

**NOAA NESDIS
CENTER FOR SATELLITE APPLICATIONS
AND RESEARCH**

**GLOBAL 4KM MULTISENSOR
AUTOMATED SNOW/ICE MAP (GMASI)**

ALGORITHM THEORETICAL BASIS DOCUMENT

March 2016

GMASI ALGORITHM THEORETICAL BASIS DOCUMENT

AUTHOR:

Peter Romanov
NOAA-CREST, City College of City University of New York
160 Convent Ave
New York, NY 10031

Peter.Romanov@noaa.gov

TABLE OF CONTENTS

	<u>Page</u>
LIST OF FIGURES	5
LIST OF TABLES.....	6
LIST OF ACRONYMS.....	7
SUMMARY	8
1 INTRODUCTION.....	9
1.1 PURPOSE.....	9
1.2 REVISIONS.....	9
1.3 DOCUMENT OVERVIEW	10
2 BACKGROUND.....	11
2.1 SNOW AND ICE REMOTE SENSING FROM SATELLITES.....	11
2.2.1 <i>Snow and Ice Mapping in the Visible and Infrared Spectral Bands</i>	11
2.2.2 <i>Snow and Ice Mapping in the Microwave</i>	15
2.2.3 <i>Combined use of Visible/IR and Microwave Data for Snow and Ice Mapping</i>	18
3 SNOW AND ICE MAPPING SYSTEM OVERVIEW.....	20
3.1 GENERAL APPROACH TO SNOW AND ICE COVER MAPPING.....	20
3.2 INSTRUMENT CHARACTERISTICS	20
3.2.1 <i>METOP AVHRR</i>	21
3.2.2 <i>GOES Imager</i>	21
3.2.3 <i>Meteosat SEVIRI</i>	22
3.2.4 <i>DMSP SSMIS</i>	23
3.3 RETRIEVAL STRATEGY	23
4 ALGORITHM DESCRIPTION	24
4.1 PROCESSING OUTLINE.....	24
4.2 ALGORITHM INPUT.....	25
4.2.1 <i>AVHRR data</i>	26
4.2.2 <i>GOES Imager data</i>	26
4.2.3 <i>MSG SEVIRI data</i>	26
4.2.4 <i>SSMIS data</i>	26
4.2.5 <i>Ancillary Data</i>	26
4.3 GMASI SNOW AND ICE COVER MAPPING ALGORITHMS	29
4.3.1 <i>Snow and ice mapping with METOP AVHRR</i>	29
4.3.2 <i>Snow and ice cover mapping with GOES Imager data</i>	36
4.3.3 <i>Snow cover mapping with METEOSAT SEVIRI</i>	37
4.3.4 <i>Snow and ice mapping using DMSP SSMIS data</i>	40
4.3.5 <i>Combining snow/ice retrievals from different sensors data</i>	43
4.3.6 <i>Recurrent gap-filling algorithm</i>	47
4.3.7 <i>Regional specifics of the algorithm implementation</i>	48
4.4 GMASI OUTPUT PRODUCT	48

5	GMASI PRODUCT VALIDATION.....	50
5.1	EVALUATION AND VALIDATION APPROACH.....	50
5.2	VALIDATION OF GMASI SNOW MAPS	50
5.2.1	Comparison with in situ data	50
5.2.2	Comparison with IMS.....	53
5.3	VALIDATION OF GMASI ICE RETRIEVALS.....	54
6	ASSUMPTIONS AND LIMITATIONS.....	55
6.1	ASSUMPTIONS	55
6.2	LIMITATIONS	55
6.3	POTENTIAL IMPROVEMENTS.....	56
7	RISKS AND RISK REDUCTION EFFORTS	57
7.1	FAILURE OF SENSORS.....	57
7.2	OTHER PROBLEMS WITH SATELLITE DATA	57
8	LIST OF REFERENCES	58

LIST OF FIGURES

	<u>Page</u>
Figure 2.1 – Spectral reflectance of natural surfaces and clouds.....	13
Figure 2.2 – Spectral microwave brightness temperature of snow and ice.....	16
Figure 2.3 – Number of SSMIS daily observations available from three DMSP satellites.....	17
Figure 4.1 – GMASI System Processing Flow.....	24
Figure 4.2 – GMASI System Detailed Processing Flow.....	25
Figure 4.3 – Land Cover Map Used by the ASI Algorithm.....	27
Figure 4.4 – ISCCP mean land surface (skin) temperature for the month of July.....	28
Figure 4.5 – Snow frequency of occurrence (left) and snow cover probability (right) maps.....	29
Figure 4.6 – Flow chart of the AVHRR spectral-based image classification algorithm.....	30
Figure 4.7 – Example of METOP-AVHRR false-color composite and snow cover map.....	33
Figure 4.8 – Coverage and examples of regional AVHRR-based snow/ice maps.....	35
Figure 4.9 – Example of GOES-Imager-based daily snow/ice map.	36
Figure 4.10 – Example of MSG SEVIRI-based daily snow map.....	38
Figure 4.11 – Map of the number of SSMIS positive snow identifications	40
Figure 4.12 – Daily global ice map derived from SSMIS DMSP data.....	42
Figure 4.13 – Flow chart of the snow cover blending algorithm.....	45
Figure 4.14 – Static boundaries delineating “potential ice” regions.....	46
Figure 4.15 – Flow chart of the procedure to combine ice retrievals	47
Figure 4.16 – GMASI daily blended snow/ice map.....	50
Figure 5.1 – GMASI snow cover maps with surface observations data overlaid.	51
Figure 5.2 – GMASI snow cover over Conterminous US with surface observations data overlaid.....	51
Figure 5.3 – Agreement of GMASI (Multisensor) and IMS snow maps to in situ snow observations.....	53
Figure 5.4 – GMASI snow cover map with IMS snow map overlaid.....	53
Figure 5.5 – Time series of the rate of agreement/disagreement between GMASI and IMS	54
Figure 5.6 – GMASI ice extent and ice extent derived from AMSR2 onboard GCOM-W1.....	55

LIST OF TABLES

	<u>Page</u>
Table 3.1 – Summary of AVHRR/3 Spectral Channel Characteristics.....	21
Table 3.2 – Summary of Spectral Channel Characteristics of GOES-N-Q Imager.....	22
Table 3.3 – Characteristics of METEOSAT SEVIRI Spectral Bands.....	22
Table 3.4 – Characteristics of SSMIS Spectral Channels used in snow and ice monitoring.....	23
Table 4.1 – Land Cover Types.....	27
Table 4.2 – Coverage and size of METOP AVHRR daily snow/ice regional maps.....	34
Table 4.3 – Coverage and size of GOES-based daily snow/ice map.....	35
Table 4.4 – Coverage and size of MSG SEVIRI-based daily snow/ice map.....	38
Table 4.5 – Characteristics of GMASI daily snow/ice product.....	47
Table 4.6 – Interpretation key for GMASI daily snow/ice product.....	48

LIST OF ACRONYMS

AMSR-E	Advanced Microwave Scanning Radiometer for EOS
AMSU	Advanced Microwave Sounding Unit
ANSA	Air-Force-NASA snow product
ATBD	Algorithm Theoretical Base Document
AVHRR	Advanced Very High Resolution Radiometer
CMG	Climate Modeling Grid
DMSP	Defense Meteorological Satellite Program
EOS	Earth Observing System
GFS	Global Forecast System
GMASI	Global Multisensor Automated Snow and Ice Mapping System
GOES	Geostationary Orbiting Environmental Satellite
GTOPO	Global Topographic Model
IMS	Interactive Multisensir Snow and Ice Mapping System
ISCCP	International Satellite Cloud Climatology Project
LSM	Land Surface Model
LST	Land Surface Temperature
McIDAS	Man computer Interactive Data Access System
METOP	Meteorological Operational Satellite
MODIS	Moderate Resolution Imaging Spectroradiometer
MSG	Meteosat Second Generation
NAS*	National Aeronautics and Space Administration
NCDC	National Climate Data Center
NCEP	National Centers for Environmental Prediction
NIC	National Ice Center
NDSI	Normalized Difference Snow Index
NDVI	Normalized Difference Vegetation Index
NESDIS	National Environmental Satellite, Data, and Information Service
NOAA	National Oceanic and Atmospheric Administration
NWS	National Weather Service
SEVIRI	Spinning Enhanced Visible and Infrared Imager
SI	Snow Index
SMMR	Scanning Multichannel Microwave Radiometer
SSM/I(S)	Special Sensor Microwave Imager (Sounder)
STAR	Center for Satellite Applications and Research
USGS	United States Geological Service
USAF	US Air Force
VIIRS	Visible/Infrared Imager Radiometer Suite

SUMMARY

This document is the Algorithm Theoretical Basis Document (ATBD) for the Global 4 km Multisensor Automated Snow and Ice Maps (GMASI) developed at the NOAA/NESDIS Center for Satellite Applications and Research (STAR). The main function of the GMASI is to routinely generate global continuous maps of snow and ice cover distribution from combined observations in the visible/infrared and in the microwave spectral bands from operational meteorological polar orbiting and geostationary satellites.

In the current configuration of the system information on the snow cover is derived from the data of Advanced Very High Resolution Radiometer (AVHRR) onboard METOP satellite, Imager instruments onboard Geostationary Operational Environmental Satellites (GOES) East and West, Spinning Enhanced Visible and Infrared Imager (SEVIRI) onboard Meteosat second Generation (MSG) and Special Sensor Microwave Imager/Sounder (SSMIS) onboard Defense Meteorological Satellite Program (DMSP) satellites. Ice cover is derived from the data of METOP AVHRR and DMSP SSMIS sensors. Both snow and ice are identified in satellite images using threshold-based decision tree image classification algorithms. Information on snow and ice cover derived from observations in the visible/infrared and in the microwave bands is then combined to allow for generation of continuous (gap-free) maps of snow and ice on a daily basis. The main output product of the system is a daily global snow and ice cover map generated on a latitude-longitude grid (Plate Carree) with a $1/25$ of a degree (or about 4 km grid cell size).

The document presents the description of the algorithms, provides examples of the product and characterizes the accuracy the derived snow and ice maps.

1 INTRODUCTION

1.1 Purpose

Snow cover is an important and highly variable component of the Earth's weather and climate system. It affects the land surface optical properties and therefore the surface energy exchange (**Dery and Brown, 2007; Robinson and Kukla, 1985**). Water accumulated in the snowpack during winter season and released during snowmelt makes the snow cover an important element of the global hydrological balance (**Arnell, 1999**). Accurate, timely and spatially detailed information on the snow cover distribution and on the snow pack properties is needed in various research and practical applications including numerical weather prediction, climate modeling, river runoff estimates and flood forecasts (e.g., **Brasnett, 1999; Tang and Lettenmaier, 2010**). Proper characterization of the snow cover properties is critical for many satellite remote sensing applications (e.g., **Loyola et al., 2011; Hsu et al, 2004**).

Satellites presents one of the key components of the global snow and ice cover monitoring system. Wide area coverage, high spatial resolution and short repeat cycle of satellite observations provide good potentials for detailed characterization of the snow and ice cover distribution and timely detection of their changes at a continental and global scales.

The Global Automated Snow and Ice Mapping System (GMASI) generates snow and ice cover maps using combined observations in the visible/infrared and in the microwave from operational meteorological satellites. The GMASI output product provides continuous (gap free) characterization of the global snow and ice cover distribution. Snow and ice maps are generated at 4 km km spatial resolution and are updated daily.

The Global Automated Snow and Ice Mapping System (GMASI) has been developed at the request of NOAA National Weather Service (NWS) and NOAA National Ice Center (NIC) to facilitate NOAA operational monitoring of snow and ice cover and to provide information on snow and ice for use in NWP models. In particular, the output of GMASI is to be used by analysts working with the NOAA Interactive Multisensor Snow and Ice System to facilitate generation of interactive snow and ice maps in the Northern Hemisphere. In the Southern Hemisphere the GMASI snow and ice maps will replace the coarse resolution US AirForce (USAF) snow cover product within the land surface model (LSM) of the Global Forecast System (GFS) operated by the National Centers for environmental Prediction (NCEP). The GMASI system has been first introduced in 2006 and was upgraded in 2010.

This document describes the algorithms incorporated in the Global Multisensor Snow and Ice Mapping System (GMASI). The document also presents the snow and ice product generated with GMASI and provides the results of the product validation and accuracy assessment.

1.2 Revisions

This version of the document was last revised in March 2016.

1.3 Document Overview

This current document contains the following sections:

- Section 1. - Introduction
- Section 2. - Background
- Section 3. - Snow and Ice Mapping System Overview
- Section 4. - Algorithm Description
- Section 5 - GMASI Product Evaluation and Validation
- Section 6. - Assumptions and Limitations
- Section 7. - Risks and Risk Reduction Efforts
- Section 8. - List of References

2 BACKGROUND

Monitoring of the Earth's cryosphere and in particular of its snow and ice cover is one of the primary applications of satellite data. Mapping of snow and ice cover from satellite observations is performed using various techniques, both interactive and automated. To identify snow and ice in satellite imagery these techniques make use of specific spectral features of snow and ice which are different from spectral features of other natural Earth's surface cover types (e.g., soil, vegetation) and from the spectral response of various atmospheric phenomena (clouds, fog, smoke, precipitation, etc.).

Identification of snow in satellite imagery by visual analysis and interpretation is the oldest snow mapping technique. Since 1972, this approach has been routinely used by the National Oceanic and Atmospheric Administration (NOAA) to generate weekly maps of snow and ice distribution in the Northern Hemisphere. In 1999, a computer-based Interactive Multisensor Snow and Ice Mapping System (IMS) was implemented to facilitate image analysis by human analysts (**Ramsay, 1998**). This improved the nominal spatial resolution of the maps from 180 km to 24 km and the temporal resolution from weekly to daily snow mapping updates. In 2004, the spatial resolution of the IMS snow products was further increased to 4 km (**Helfrich et al., 2007**).

Although the interactive approach to snow and ice map generation has proved to be accurate and robust, it is labor intensive and is affected by subjectivity of satellite image interpretation by individual human analysts. Interactively generated snow and ice maps are difficult to reprocess. This fact complicates generation of consistent time series of the product for climatological analyses. Therefore a wider interest is attracted to automated algorithms for mapping snow and ice cover from on satellite observations. In contrast to interactive snow and ice mapping techniques (similar to IMS), automated algorithms can better utilize the advantages of satellite observations, including high spatial resolution, multispectral sampling, and a frequent repeat observation cycle.

The two principal techniques most actively used in the automated snow and ice identification and mapping are based correspondingly on passive observations in the visible/infrared and microwave spectral bands. A number of algorithms have been proposed where satellite observations in the visible/infrared and in the microwave are combined to achieve more accurate characterization of the snow and ice cover. The latter approach is utilized in the NESDIS Global Automated Snow and Ice Mapping System (GMASI). For mapping snow and ice cover GMASI system uses combined observations in the optical and microwave spectral bands conducted from polar orbiting and geostationary operational meteorological satellites.

This section presents a short review of physical principles of snow and ice detection in the visible/infrared and microwave and a review of particular algorithms developed and applied to satellite data for snow and ice mapping.

2.1 Snow and Ice Remote Sensing from Satellites

2.2.1 Snow and Ice Mapping in the Visible and Infrared Spectral Bands

Snow Mapping

Automated identification of snow is based on a specific spectral reflectance signature exhibited by snow-covered land surface. The reflectance of snow drops from high values, up to 90-95%, in the visible spectral band to low values below 20% in the shortwave and in the middle infrared spectral band (see Figure 2.1). This spectral pattern of snow cover reflectance is different from spectral reflectance of most natural land surface cover types (e.g., soil, water vegetation) which typically appear much “darker” in the visible band. In the far infrared spectral band, snow emits thermal radiation close to that of a blackbody and thus its brightness temperature as observed by the satellite sensor depends mainly on the physical temperature of the top thin layer of the snow pack. In these wavelengths, the snow brightness temperature is relatively low, which is also useful information for snow identification.

Most clouds are opaque in the visible and infrared spectral bands. Liquid-phase clouds typically exhibit high reflectance both the visible and in the shortwave infrared bands. High reflectance in the visible band along with colder infrared brightness temperature discriminates clouds from snow-free land surface, whereas their high reflectance in the shortwave infrared differentiates clouds from the snow-covered land surface.

Most current instruments onboard polar orbiting and geostationary satellites collect observations in spectral regions centered in the visible at around 0.6 μm , the shortwave-infrared at 1.6 μm , middle infrared at 3.7 μm - 3.9 μm , and the thermal infrared at 10 μm -12 μm . Observations in these spectral bands are generally sufficient to distinguish snow from most clouds and from the snow-free land surface and therefore can be used to map the snow cover distribution.

Generation of a map of snow cover distribution from satellite observations in the visible and infrared spectral bands implies attributing every land pixel of satellite image to one of three categories, snow-cover, snow-free land surface and cloud. Automated (or unsupervised) algorithms to identify snow usually incorporate a set of threshold tests or criteria that utilize satellite-observed reflectance and brightness temperature values in the spectral bands mentioned above as well as various spectral indices. Spectral indices are utilized to characterize the spectral gradient of the scene reflectance or brightness temperature and can be defined as ratios, differences or normalized differences of the observed reflectance or brightness temperatures at two, or, sometimes, three, wavelengths. As an example, in the algorithm described in **Romanov et al. (2000)** snow is primarily identified using a snow index (**SI**), defined as a simple ratio of the TOA reflectance in the visible (R_{vis}) and in the middle infrared (R_{mir}). This snow identification algorithm has been developed to identify snow cover from observations of the Imager sensor onboard Geostationary Operational Environmental Satellites (GOES) satellites. The visible and middle infrared spectral bands of the Imager sensor are centered correspondingly at 0.6 μm and 3.9 μm . Since the reflectance of snow remains very low in both the middle infrared and in the shortwave infrared spectral range, a similar index where R_{mir} , is replaced by the observed reflectance in the shortwave infrared (R_{sir}) can also be used in snow detection schemes.

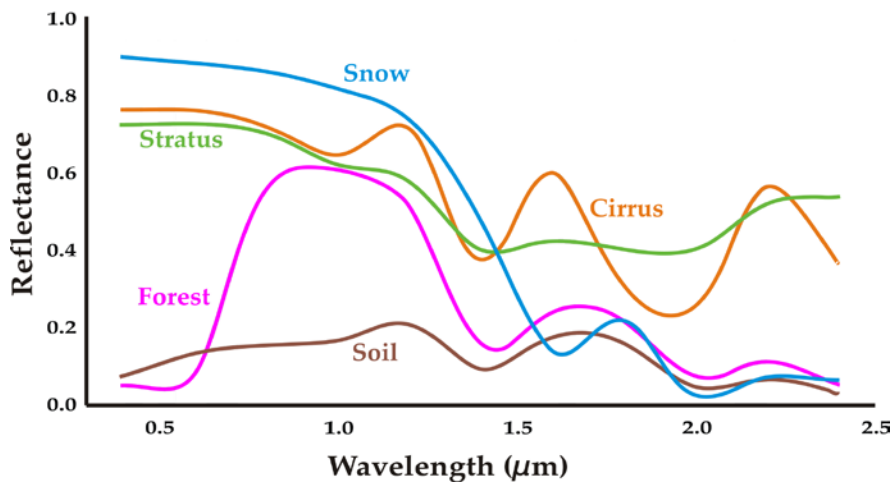


Figure 2.1 – Spectral reflectance of natural surfaces and clouds

The snow detection algorithm of **Hall et al. (2002)** uses the normalized difference between TOA reflectance observed with the Moderate Resolution Imaging Spectroradiometer (MODIS) onboard NASA Terra and Aqua satellites in the visible spectral band at 0.6 μm (R_{vis}) and in the shortwave infrared spectral band at 1.6 μm (R_{sir}). The index is called the Normalized Difference Snow Index (NDSI) and is expressed as

$$NDSI = (R_{vis} - R_{sir}) / (R_{vis} + R_{sir})$$

Clouds and snow-free land surfaces typically exhibit lower values of SI and NDSI than snow covered land. In the snow mapping algorithm of **Hall et al. (2002)**, cloud-free pixels having $NDSI > 0.4$, a visible reflectance of over 11%, and infrared brightness temperature below 283K are classified as snow-covered.

There is a number of factors complicating snow identification in satellite imagery and hampering generation of accurate maps of the snow cover distribution. One of these factors is vegetation which masks snow cover on the ground surface reducing the visible reflectance of the scene. This effect is the strongest in densely forested areas where most misses of snow cover in satellite snow products occur. To account for the vegetation cover effects on the snow reflectance and to improve snow identification in forests, snow identification some algorithms incorporate the Normalized Difference Vegetation Index (NDVI) (e.g., **Hall et al, 2002**):

$$NDVI = (R_{nir} - R_{vis}) / (R_{nir} + R_{vis}),$$

where R_{nir} is the scene reflectance in the near infrared spectral band.

Clouds of certain types may look very similar to snow in the visible and shortwave infrared spectral bands and thus may be confused with the snow cover by the image classification algorithm. If

available, additional detailed spectral observations in the 15 micron band of CO₂ may be used to improve cloud identification. Cloud identification can also be improved if a good estimate of the land surface temperature is available. Estimate of the land surface temperature could be obtained from a numerical weather prediction model (e.g., **Feijt, et al., 2000**) or from available land surface temperature climatology.

Cloud obscuration presents one of the primary problems in snow identification with satellite observations in the visible/infrared and a major weakness of corresponding snow map products. Inability of visible/infrared sensor to “see” through clouds result in gaps in the derived daily snow cover maps and hampers timely identification of changes in the snow cover distribution with satellite data. This problem can be partially alleviated by using observations from geostationary satellites.

Most current imaging instruments onboard geostationary satellites provide observations in the visible, middle-infrared, and thermal infrared spectral bands and thus also allow for an automated snow cover identification and mapping. In contrast to polar orbiting satellites which typically provide one daytime observation per day, observations from geostationary satellites are available at much frequent, 15-30 minutes, time interval. Frequent observations increase the chance to observe the land surface cloud-clear during the day and thus reduce cloud-caused gaps in the daily snow cover product. An algorithm to identify and map snow cover with observations from GOES data is presented in **Romanov et al., 2003**. A number of snow mapping algorithm have been developed to identify snow cover and generate snow maps from observations of Spinning Enhanced Visible and Infrared Imager (SEVIRI) onboard Meteosat Second Generation (MSG) satellites (.e.g., **Romanov & Tarpley, 2006, deWildt et al. 2007**).

Ice Mapping

The spectral reflectance of thick ice is similar to the reflectance of snow. Therefore algorithms to identify ice cover have much in common with algorithm used to identify and map snow. Ice is typically differentiated from open water by larger NDSI value, high visible reflectance and low infrared brightness temperature.

Most automated algorithms to identify ice cover have been developed to the data from polar orbiting satellites. **Zibordi and VanWoert (1993), Zibordi et al. (1995), Key et al. (2001) and Wang & Key (2001, 2005)** have used observations from the Advanced Very High Resolution Radiometer (AVHRR) onboard NOAA satellites to map the ice cover distribution. Since 2000, ice mapping is routinely performed with data from the Moderate Resolution Imaging Spectroradiometer (MODIS) onboard the Terra and Aqua satellites (**Riggs et al. 1999, Hall et al. 2004, Drue & Heinemann 2005**). A technique to derive ice cover from MSG SEVIRI data has been proposed by **Temimi et al. (2011)**. To better discriminate ice from clouds the latter algorithm examines temporal variation of the scene spectral response during the day. Large diurnal variations of the scene reflectance and/or infrared brightness temperature are indicative of clouds in the instrument field of view. Optical measurements have also been applied to study ice phenology over small inland water bodies, where microwave measurements are ineffective (e.g. **Latifovic and Pouliot, 2007**).

Unlike microwave data, application of satellite observations in the visible and infrared is limited to daytime clear-sky conditions. Therefore, they are less effective in monitoring large masses of ice in the polar regions. However, their finer spatial resolution, of the order of 1 km or less, gives them an advantage over microwave data in mapping and monitoring ice cover over small inland water

bodies, lakes and even some rivers. Visible and infrared data are also more effective in detecting ice along coastal lines.

Identification of thin ice may present a problem since thin ice exhibits low reflectance in the visible spectral band and this can be distinguished from the ice-free water only by the infrared brightness temperature. Proper distinguishing ice from clouds may be complicated by the fact that some clouds may exhibit a spectral response in the visible and infrared similar to ice.

2.2.2 Snow and Ice Mapping in the Microwave

Snow Mapping

Observations in the passive microwave have been used to monitor snow cover since mid-1970s. Dry snow cover presents a scattering medium in the microwave spectral bands. It scatters and, hence attenuates radiation emitted by the ground surface. Within the spectral range of 10 GHz to 100 GHz typically used for satellite monitoring of land surface features the scattering effect associated with the snow cover increases with increasing frequency of microwaves. As a result, the spectral emissivity and, correspondingly the brightness temperature of snow covered scenes decrease with increasing frequency of radiation (see Fig 2.2). In contrast to snow the emissivity of bare soils is typically spectrally neutral (**Grody & Basist, 1996**). The specific spectral gradient of brightness temperature inherent to snow-covered scenes is used as the primary feature to distinguish snow from snow-free land surface.

Some potential exists to estimate snow depth and snow water equivalent from microwave observations, however the accuracy of these estimates is poor and errors typically exceed 50% (Foster et al, 2005). Time series of snow extent at regional, continental and global scale have been derived from the data of the Scanning Multichannel Microwave Radiometer (SMMR), flown on the Nimbus-7 satellite, Special Sensor Microwave/Imager (SSM/I) on the U.S. Defense Meteorological Satellite Program (DMSP) satellites and Advanced Microwave Scanning Radiometer (AMSR-E) onboard Aqua.

Except of the high frequency band centered at 85-89GHz satellite observations in the microwave are practically unaffected by most types of clouds. In contrast to the visible/infrared techniques snow retrievals in the microwave do not require daylight. Known limitations of the microwave measurements include their coarse, about 25-50 km, spatial resolution and poor sensitivity to shallow and melting snow (**Walker and Goodison, 1993**). The latter weakness results in underestimation of the snow extent in spring and fall and frequent snow misses during mid-winter snow melt events. The spectral response of cold rocks in the microwave may be similar to the one of snow (**Grody and Basist, 1996**). As a result microwave snow cover products often overestimate the snow extent in mountainous regions. Another snow identification problem is associated with precipitation, and with mixed land/water scenes. In both cases the spectral response in the microwave may be similar to the one of snow.

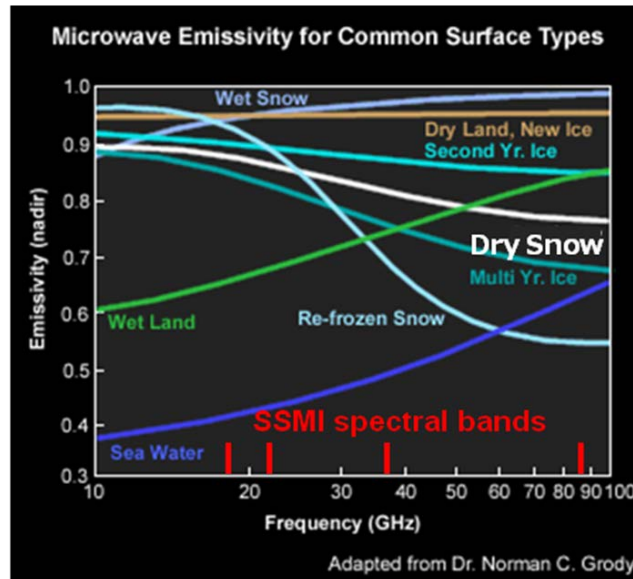


Figure 2.2 – Spectral microwave brightness temperature of snow and ice

Spectral features used in the snow remote sensing algorithms differences of the brightness temperatures at 19, 22, 37, and 87 GHz both at vertical and horizontal polarizations. The difference between the brightness temperature observed at 19 and 37 GHz is most sensitive to snow packs and is utilized in most current microwave snow identification algorithms. Algorithms utilizing this feature have been used to derive maps of snow cover from observations of Special Sensor Microwave Imager (SSM/I) onboard Defence Meteorological satellite program (DMSP) satellites (**Armstrong and Brodzik, 2001, Derksen et al., 1998, Royer et al., 2010**), Advanced Microwave Sounding Unit (AMSU) onboard NOAA and METOP polar orbiting satellites (**e.g., Kongoli et al., 2007**) and from Advanced Microwave scanning Radiometer (AMSR-E) onboard Terra and Aqua satellites (**Kelly et al., 2003, Tedesco and Wang, 2006**). A robust and accurate technique to identify snow cover has been developed by Grody and Basist (1996). The algorithm first identifies “scattering” surfaces using brightness temperature spectral gradient values derived from observations at 22 and 85 GHz and at 19 and 37 GHz correspondingly and then employs a set of additional threshold tests to discriminate the actual snow from precipitating clouds, cold desert scenes and frozen ground. The difference of microwave brightness temperature observed in 19 GHz band at vertical and horizontal polarization is further used to identify glacial ice. The **Grody and Basist (1996)** technique is currently implemented at NOAA to routinely generate snow and ice maps from the data of SSM/I and newer generation Special Sensor Microwave Imager/Sounder (SSMIS) onboard DMSP satellites.

An important feature of SSMIS is availability of observations from multiple satellite platforms. Since the end of 1990s, SSM/I and later on SSMIS observations were conducted from three or more satellites at the same time yielding from 4 to 6 daily “looks” in mid- and high latitude regions (see Fig.2.3). Information on the temporal variation of the scene response provided by multiple daily observations in the microwave helps to better distinguish snow cover from precipitating clouds which may exhibit a spectral response in the microwave similar to snow.

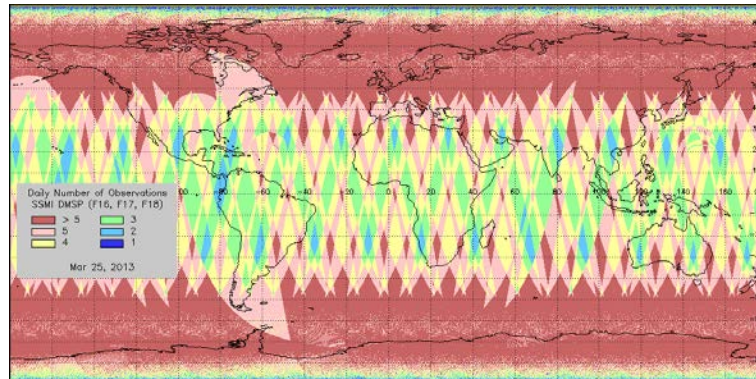


Figure 2.3 – Number of SSMIS daily observations available from three DMSP satellites

Ice Mapping

Satellite passive microwave observations present the most reliable and the most widely used tool for large scale monitoring of ice cover properties. In the spectral range from ~5 GHz to ~94 GHz covered by many satellite microwave sensors emissivity of open water, and, correspondingly, its brightness temperature increases with frequency whereas emissivity and brightness temperature of ice remain unchanged or decrease with frequency. The difference in the spectral gradient of the brightness temperature is the primary feature used to distinguish between the ice and open water in satellite passive microwave imagery. Since atmospheric effects progressively increase at frequencies of 50 GHz and larger most ice identification algorithms utilize satellite observations in the 19 and 37 GHz spectral bands at vertical and horizontal polarization. Another feature utilized to differentiate between ice and open water is the polarization difference. For open water scenes the difference between emissivity (and, hence, brightness temperature) at vertical and horizontal polarization is noticeably larger than the corresponding difference over ice. The contrast between polarization difference of water and ice increases with decreasing frequency. Increasing extent of the sea ice within the instrument field of view causes gradual change of the microwave spectral brightness temperature. This latter feature is actively used to estimate the sea ice concentration from satellite observations in the microwave.

Automated algorithms to derive ice concentration and ice extent have been developed and applied to observations of Scanning Multichannel Microwave Radiometer (SMMR) onboard Nimbus-7, Special Sensor Microwave Imager (SSM/I) and Special Sensor Microwave Imager/Sounder (SSMIS) instruments onboard Defense Meteorological Satellite Platform (DMSP) satellites, Advance Microwave Scanning Radiometer (AMSR-E) onboard Aqua satellite (e.g., **Comiso et al, 1997**, **Ferraro et al, 1996**). Since 2000 Ice concentration has been routinely monitored with the data from Advanced Microwave Sounding Unit (AMSU) onboard NOAA satellites. Since this latter instrument lacks polarized spectral bands, ice is identified from only the spectral response of a scene (**Kongoli, 2011**).

The two most widely used techniques to identify ice and derived the ice concentration using satellite observations in the microwave are the ones developed by **Cavaliere et al (1994)** and known as “NASA Team Algorithm” and by **Comiso (1995)**, known as “Bootstrap Algorithm” Both algorithms were applied to observations of DMSP SSM/I. Enhanced versions of both algorithms

have been used to derive the sea ice concentration in Arctic and Antarctic from observations of AMSR-E instrument onboard Aqua satellite (**Cavalieri and Comiso , 2000**).

To identify sea ice and determine its concentration the NASA Team algorithm employs the normalized brightness temperature gradient in 37 and 19GHz spectral bands at vertical polarization (or spectral gradient ratio) and the normalized polarization difference at 19GHz (or polarization ratio). For the AMSR-E data processing the NASA Team algorithm was modified by adding observations in the 85 GHz spectral band to better identify thin ice and filter out atmospheric effects. The Bootstrap algorithm estimates the ice concentration from a bootstrap approach using multidimensional cluster analysis of brightness temperature values in 19 GHz and 37GHz spectral bands. Both techniques compare well in detecting the ice cover, but may exhibit up to 25-30% difference in the derived ice concentration (**Comiso et al., 1997**).

All weather and day/night capabilities of microwave observations make passive microwave remote sensing attractive for monitoring sea ice in high latitude areas where lack of daylight and persistent cloud cover are common features. The principal weakness of passive microwave sensors is their coarse spatial resolution which ranges generally from 10-15 km to 100-150 km. In most existing satellite microwave instruments the spatial resolution of sensors varies with frequency. These two issues hamper the use of microwave measurements for ice detection and mapping over small lakes and in the vicinity of coastal lines (**Cavalieri et al, 1997**).

2.2.3 Combined use of Visible/IR and Microwave Data for Snow and Ice Mapping

To satisfy the needs of NWP, climate, hydrological and other environmental models information on the snow cover state should be accurate, timely, spatially detailed and continuous. Most operational mesoscale and global models where information on the snow cover is used as an external input require at least daily updates of the status of the snow cover at the spatial resolution of one to several kilometers (e.g., **Pullen et al, 2011; Hyvarinen et al., 2009**). None of the two automated satellite-based remote sensing techniques, passive microwave and visible/infrared, and corresponding products derived with any one stand alone technique satisfies the model needs. Snow/ice products derived from observations in the visible/infrared are accurate and spatially detailed but have gaps in the area coverage due to clouds. Microwave products may not have gaps in the area coverage owing to their all-weather capability but their spatial resolution is too coarse to adequately reproduce the snow cover distribution, particularly in alpine regions, and the ice cover over small inland water bodies. Potentials to improve mapping and monitoring of snow and ice cover are associated with the use of blending or fusion techniques which combine satellite observations of the snow cover in the optical/infrared and in the microwave bands. The principal objective of these techniques is to generate continuous (gap free) maps of the snow and ice cover distribution on a daily basis at the best attainable spatial resolution.

Most existing blending algorithms utilize a simple approach where gaps in the daily snow product derived from one sensor are filled in with retrievals from the other instrument (e.g., **Liang et al., 2008, Gao et al., 2010**). Some of the proposed blending techniques rely primarily on the microwave snow retrievals. In particular, in **Armstrong et al., (2003) and Armstrong et al., (2004)** 8-day composited maps of snow water equivalent derived from SSM/I complemented by MODIS-based 8-day composited snow cover maps to produce an 8-day blended, 25 km resolution global map of snow cover distribution. In this technique optical MODIS data were used to compensate for possible omissions of shallow or melting snow in the MW-based snow product. Most often in the blending algorithms the priority is given to optical snow estimates owing to their better accuracy and

higher spatial resolution. In these techniques microwave retrievals fill in gaps in the optical products in cloudy and polar night conditions. This approach where optical data are considered the primary source of information on the snow cover and are complemented with microwave snow retrievals is implemented in particular in the blending algorithm known as Air-Force-NASA or ANSA. The ANSA algorithm combines snow retrievals from two sensors, MODIS and AMSR-E onboard NASA Earth Observing satellites (EOS) Terra and Aqua (**Foster et al., 2011**) to generate a daily continuous snow cover map over Northern Hemisphere produced at 25 km spatial resolution. Generation of this product was terminated in 2001 due to the failure of AMSR-E instrument.

As compared to the solely microwave snow product, the combined product where part of microwave retrievals is replaced with more accurate optical retrievals has a clear potential to better reproduce the snow cover distribution. Still the effect of errors of the microwave retrievals incorporated in the combined product may be substantial. Reduction of the effect of these errors can be achieved by utilizing a larger number of available optical observations, particularly, by using geostationary satellite data, and by more conservative and cautious use of microwave snow retrievals. This approach has been implemented in the algorithm of **Romanov et al. (2000)** which involved observations from geostationary satellites, combining and consistency testing of snow retrievals from several microwave sensors and application of a snow cover climatology-based algorithm when merging optical and microwave snow products. The principal difference of this approach from the one of **Foster et al. (2007)** is that MW observations classified as “snow-free land surface” are disregarded in the blending technique due to frequent omission of melting snow and shallow snow in the MW product. MW snow retrievals over mountains are also disregarded because of their tendency to confuse cold rocky surfaces with snow and thus to overestimate snow cover extent in high-altitude areas. Recurrent gap-filling technique is applied in this algorithm to achieve continuity of the derived daily snow cover maps.

The technique presented in **Romanov et al (2000)** has been used at NOAA for routine automated mapping and monitoring snow cover since 2002. The basic approach to combining satellite observations in the visible/infrared and in the microwave has been incorporated in the global system for snow and ice cover monitoring operated by NOAA since 2006.

3 SNOW AND ICE MAPPING SYSTEM OVERVIEW

3.1 General Approach to Snow and Ice Cover Mapping

The principal approach to the snow and ice cover mapping within the GMASI system consists in the synergy of satellite observations in the visible/infrared and in the microwave spectral bands both from operational meteorological polar orbiting and geostationary satellites. Combined use of satellite observations in the visible/infrared and in the microwave allows for the most accurate and detailed snow and ice mapping and timely reproduction of the global snow and ice cover variations.

Within the system daily observations from all satellite sensors are processed separately and individual daily maps of snow and ice cover are derived. Snow and ice in satellite imagery are identified using decision-tree threshold-based image classification algorithms. Several auxiliary datasets are used to improve the classification accuracy and make snow and ice identification more reliable. At the next step of the data processing information on snow and ice distribution derived from different satellite sensors (both visible/infrared and microwave) is combined to provide the best possible area coverage with the current day satellite observations. Lastly a recurrent gap-filling technique is applied to achieve full continuity of the daily snow and ice map and the final snow and ice map is derived. The output product presents a global, continuous (gap-free) map of snow and ice cover distribution. Maps are derived on a daily basis at 4 km spatial resolution.

3.2 Instrument Characteristics

To generate snow and ice cover maps the GMASI system acquires and processes data from several sensors onboard operational meteorological polar orbiting and geostationary satellites. The current (as of February 2014) list of sensors used in the system includes:

- Advanced Very High Resolution Radiometer (AVHRR) onboard METOP-A satellite
- Imager onboard Geostationary Operational Environmental Satellite-East (GOES-EAST)
- Imager onboard Geostationary Operational Environmental Satellite-West (GOES-WEST)
- Spinning Enhanced Visible and Infrared Imager (SEVIRI) onboard Meteosat-8
- Special Sensor Microwave Imager/Sounder (SSMIS) onboard Defense Meteorological Satellite Program (DMSP) satellites F-16, -17, and -18

Prior to November 2010 NOAA-17 AVHRR data were used in the system instead of METOP AVHRR the system and DMSP SSMI data were used instead of SSMIS.

Characteristics of all instruments incorporated in the GMASI system to map snow and ice cover are presented below.

3.2.1 METOP AVHRR

The AVHRR instrument is a cross-track scanning radiometer providing observations in the visible and infrared spectral range. The AVHRR instrument onboard METOP satellite is the third generation AVHRR instrument. It has five channels that cover 6 spectral bands, as Channel 3 is switched from observations in the middle infrared at night to the shortwave infrared during daytime.

METOP satellite is a polar orbiting satellite. AVHRR instrument onboard METOP provides global observations at 1.1 km spatial resolution. The METOP altitude is about 800 km. At this altitude the AVHRR swath width comprises about 2400 km. With this swath width AVHRR provides a complete coverage of the globe two times a day. The time of METOP daytime overpass is around 9.30 AM local time.

At the time of the last update to the document AVHRR observations were available from two METOP satellites, METOP-A launched in October 2006 and Metop-B launched in September 2012. Only Metop-A AVHRR data were used in the system.

Table 3.1 – Summary of AVHRR/3 Spectral Channel Characteristics

Parameter	Ch. 1	Ch. 2	Ch. 3A	Ch. 3B	Ch. 4	Ch. 5
Spectral Range (µm)	0.58-0.68	.725-1.0	1.58-1.64	3.55-3.93	10.3-11.3	11.5-12.5
Resolution (km)	1.09	1.09	1.09	1.09	1.09	1.09

3.2.2 GOES Imager

The Imager instrument onboard GOES N-Q satellites is a five channel (one visible, four infrared) imaging radiometer designed to sense radiant and solar reflected energy from sampled areas of the Earth. At the time of the last update of the Document (October 2013) the operational GOES satellites were GOES-13(N) as GOES-East and GOES-15(P) as GOES-West. The two satellites , GOES-East and GOES-West are positioned correspondingly at 75° W and 135° W.

Imager instruments onboard GOES satellites provide full scan observations at the nominal time step of 30 min. The spatial domain of the instrument observations is generally limited to 65-70° N and S. Imager observations from GOES East cover the eastern and central part of North America and South America whereas observations from GOES West cover the central and western part of North America.

Information on the spectral band of GOES Imager instrument is given in Table 3.2. Observations in the visible (band 1), shortwave infrared (band 2) and in the infrared band 4 are used for mapping

snow and ice cover. The spatial resolution in all bands shown in Table 3.2 corresponds to the nadir view.

Table 3.2 – Summary of Spectral Channel Characteristics of GOES-N-Q Imager

Parameter	Ch. 1	Ch. 2	Ch. 3	Ch. 4	Ch. 5
Spectral Range (μm)	0.55-0.75	3.8-4.0	6.50-7.00	10.2-11.2	12.9-13.7
Resolution (km)	1	4	8	4	4

3.2.3 Meteosat SEVIRI

The SEVIRI instrument onboard Meteosat Second Generation (MSG) satellite is a 12- channel imaging radiometer. At the time of the last update of the Document (October 2013) the operational MSG satellite positioned at 0°E was Meteosat-10.

SEVIRI instrument onboard MSG satellites provide full scan observations with the image repeat cycle of 15 minutes. Similar to other geostationary satellites the spatial domain of MSG SEVIRI is limited to 65-70° N and S. SEVIRI observations from MSG positioned at 0°E cover Africa, and the western part of Eurasia up to about 50-55°E.

Information on the spectral bands of MSG SEVIRI instrument is given in Table 3.3. Observations in bands 1,2,3 and 9 are used for mapping snow and ice cover. The spatial resolution of all bands in Table 3.3 is given for the nadir view.

Table 3.3 – Characteristics of METEOSAT SEVIRI Spectral Bands

Band number	1	2	3	4	5	6	7	8	9	10	11	HRV*
Spectral Range, (μm)	0.56-0.71	0.74-0.88	1.50-1.78	3.48-4.36	5.35-7.15	6.85-7.85	9.38-9.94	8.30-9.10	9.80-11.8	11.0-13.0	12.4-14.4	0.6-0.9
Resolution (km)	3	3	3	3	3	3	3	3	3	3	3	1

*High Resolution Visible band

3.2.4 DMSP SSMIS

The first Special Sensor Microwave Imager/Sounder (SSMIS) sensor was launched in October 2003 onboard the DMSP F-16 platform. It is a passive conically scanning microwave radiometer with a swath width of about 1700 km which measures outgoing microwave radiation in 24 bands from 19 to 183 GHz. At some frequencies polarized observations are performed. Most of SSMIS bands are used for atmospheric monitoring. The list of bands used in snow and ice retrievals is presented in Table 3.4.

As of the time of the last update to this Document SSMIS observations were available from three DMSP satellites, F-16 launched in October 3002, F-17 launched in November 2006 and F-18 launched in October 2009.

Table 3.4 – Characteristics of SSMIS Spectral Channels used in snow and ice monitoring

Band number	12	13	14	15	16	17	18
Frequency (GHz)	19.3	19.3	22.2	37.0	37.0	91.6	91.6
Polarization	H	V	V	H	V	V	H
Footprint size (km)	44.8	44.8	44.8	27.5	27.5	13.2	13.2

3.3 Retrieval Strategy

Within the system data from each individual satellite sensor collected during the day are processed separately and information on snow and ice cover is derived. Snow and ice retrievals from different sensors are then combined. Map grid cells that could not be reliably classified with satellite observations acquired during the current day are filled in with the most recent in time valid retrieval results. This recurrent algorithm (or gap-filling technique) ensures generation of continuous (gap free) snow and ice cover maps on a daily basis.

The system utilizes auxiliary datasets which are used to identify and eliminate questionable snow and ice retrievals. A land/water mask is incorporated in the algorithm to limit snow and ice retrievals correspondingly to only land and water surfaces.

Blended daily snow and ice maps over the Northern and Southern Hemisphere are generated separately and are then combined to achieve the full global coverage. There is a number of regional differences in the snow and ice mapping algorithms. Some regions of the Earth are assumed either permanently snow free or permanently snow covered. No snow cover retrievals are performed over these regions. The primary output of the system is a global continuous daily map of snow and ice cover distribution generated on a latitude-longitude grid with 0.04 degree grid cell size (or approximately at 4 km spatial resolution) with every land grid cell of the map labeled as

“snow-free land” or “snow cover” and every map grid cell over water surface labeled as “clear water” or “ice cover”.

The system is scheduled to continuously collect satellite observations during. For a daily snow and ice map satellite observations acquired within a 24-hour period (0000-2359UTC) are used. The main processing of satellite observations and snow/ice map generation is conducted in the beginning of the next day. The output daily snow and ice map typically becomes available at 1100-1200UTC the next day.

4 ALGORITHM DESCRIPTION

4.1 Processing Outline

The general processing flow of the Global Multisensor Automated Snow and Ice Mapping System is shown in Figure 4.1.

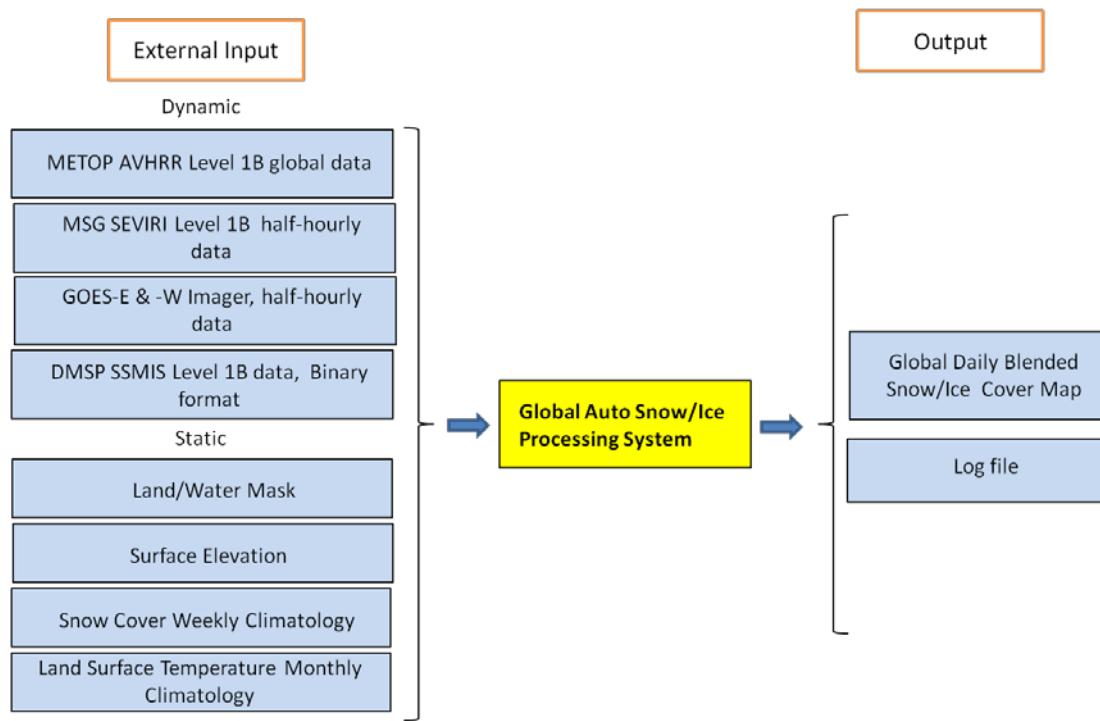


Figure 4.1 – GMASI System Processing Flow

GMAI generates the blended daily global snow and ice cover map at 4 km spatial resolution. The blended daily snow and ice cover map presents a gridded image where every grid cell is attributed to one of four categories: “snow-free land surface”, “snow”, “ice-free water” and “ice”. The input data the system uses to generate the products include observations from METOP AVHRR, GOES-East and -West Imager, MSG SEVIRI and from DMSP SSMIS instruments along with the land/water mask, surface elevation data, the land surface temperature climatology and the climatic snow occurrence dataset.

Within the system data from all sensors are processed separately and individual snow and ice maps are generated. Information on snow and ice from individual sensors is then combined and complemented with the first guess (which is the previous day snow/ice mapping results) to generate a blended daily snow and ice cover map (see Fig 4.2)

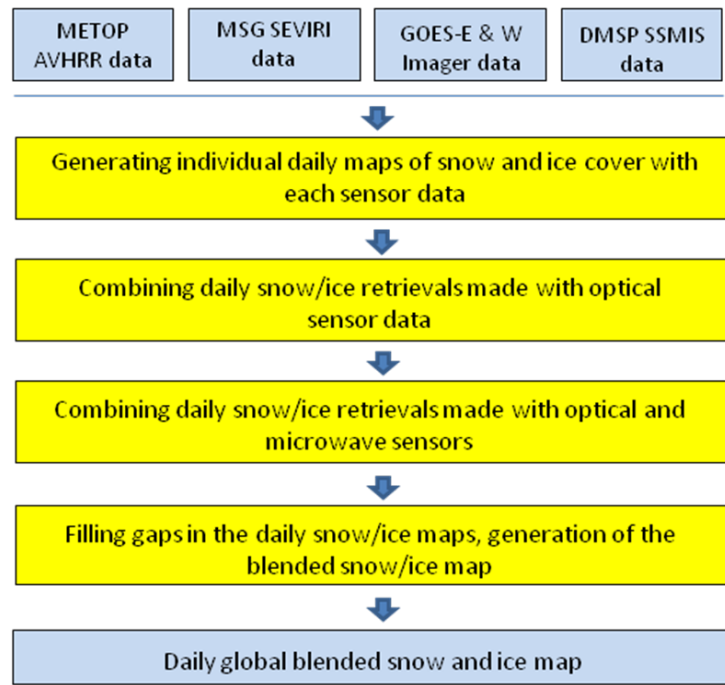


Figure 4.2 – GMAI System Detailed Processing Flow

4.2 Algorithm Input

4.2.1 AVHRR data

The algorithm incorporates METOP AVHRR level 1b swath data in McIDAS AREA format. These data are acquired from the FRAC dataset of NOAA/NESDIS McIDAS PLR server (IP: 140.90.213.159). Within the system all AVHRR daytime observations in bands 1, 2, 3a and 4 (see Table 3.1) from all orbits are processed and used for mapping global snow and ice cover.

4.2.2 GOES Imager data

All daily daytime images at 30 min interval from GOES-East and GOES-West satellites in bands 1,2 and 4 (see Table 3.2) are processed and applied for mapping snow and ice cover within the two satellites domain. Observations from GOES-East and -West are used to map snow and ice correspondingly east and west of 100⁰W. GOES level 1b data are acquired in McIDAS AREA format.

4.2.3 MSG SEVIRI data

Mapping of snow and ice cover with MSG SEVIRI data is performed with observations in bands 1,2,3 and 9 (see Table 3.3). To reduce the processing time every other of SEVIRI 15-minute images is processed. MSG SEVIRI level 1b data are acquired in McIDAS AREA format.

4.2.4 SSMIS data

The algorithm uses DMSP SSMIS level 1b swath data in binary format. This data are acquired from TDRR dataset of NOAA/NESDIS satepsdist server (IP: 140.90.213.159). Information on the ice cover is derived from SSMIS data using observations in bands 12-18 at frequencies of 19, 22 and 37 GHz and 91 GHz (see Table 3.4)

4.2.5 Ancillary Data

The ancillary data for the GMASI processing system include land/water mask, surface elevation data, land surface temperature climatology data and snow cover occurrence climatology data.

Land/water mask

The global land cover map is needed to limit snow retrievals to land areas and ice retrievals to the sea only. The land cover map used in the system (see Figure 3.3) has been generated from 1-km land cover map produced by University of Maryland Geography Department (online at <http://www.glcfc.umd.edu/data/landcover/>). Table 4.1 lists the land cover code in the land cover map.

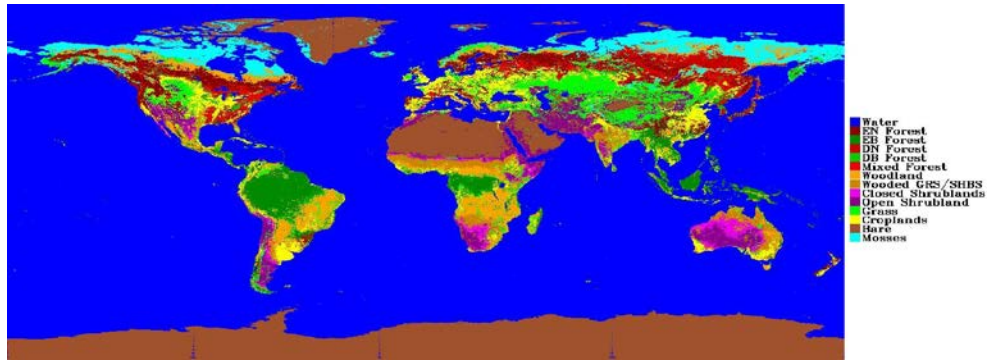


Figure 4.3 – Land Cover Map Used by the ASI Algorithm

Table 4.1 – Land Cover Types

Code	Land Cover Type	Code	Land Cover Type
0	Water	7	Wooded Grasslands/Shrubs
1	Evergreen Needleleaf Forests	8	Closed Bushlands or Shrublands
2	Evergreen Broadleaf Forests	9	Open Shrublands
3	Deciduous Needleleaf Forests	10	Grasses
4	Deciduous Broadleaf Forests	11	Croplands
5	Mixed Forests	12	Bare
6	Woodlands	13	Mosses and Lichens

Forest cover fraction

The global forest cover fraction map is used in the snow blending algorithm to determine densely vegetated areas where snow retrievals in the visible and infrared bands may fail. Information on the forest fraction was obtained from the global percent tree cover dataset produced on a 1-km resolution grid by University of Maryland Department of Geography (online at <http://www.glcg.umd.edu/data/treecover/>).

Surface elevation

Surface elevation data is needed to properly adjust the available coarse spatial resolution land surface temperature climatology for variable elevation. Elevation data are also in the incorporating the snow cover occurrence climatology and to distinguish mountain and plain areas when determining the geographical limits of application of microwave observations. USGS GTOPO30 model data are used as a source for surface elevation. The data are available online at http://eros.usgs.gov/#/Find_Data/Products_and_Data_Available/GTOPO30.

Land Surface Temperature Climatology

Land surface temperature climatology is based on the data of the International Satellite Cloud Climatology Project (ISCCP). Monthly mean surface temperature is specified within 5x5 degree grid cells. Data are available from ISCCP anonymous ftp site at <ftp://isccp.giss.nasa.gov/pub/data/surface/>. As an example, Figure 4.4 presents global mean temperature for the month of July.

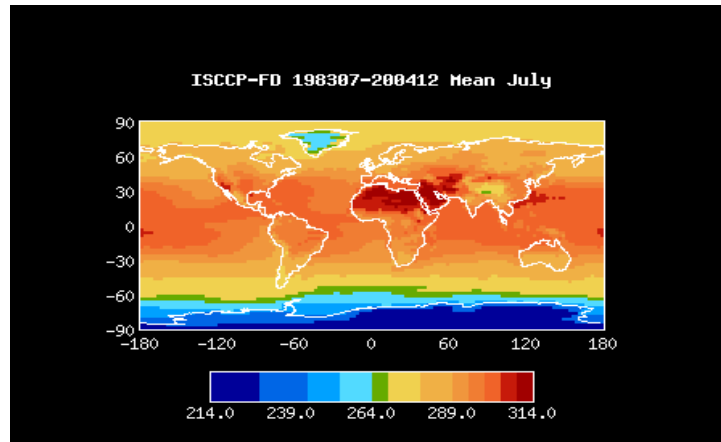


Figure 4.4 – ISCCP mean land surface (skin) temperature for the month of July

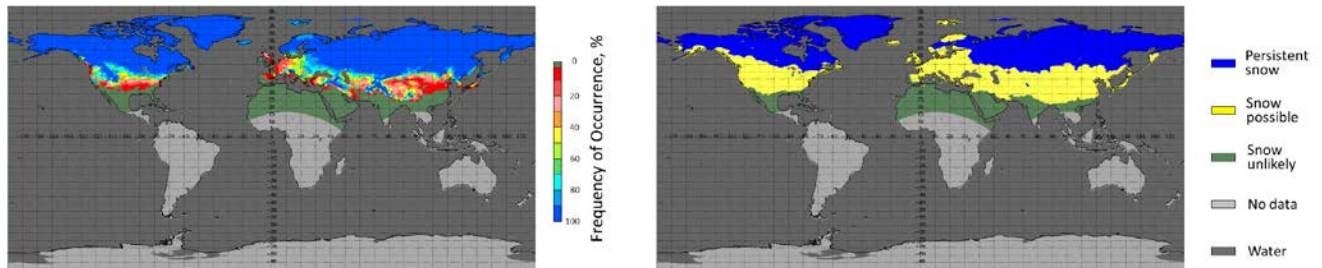
Snow cover occurrence climatology

In the system information on the snow cover occurrence is used when combining snow retrievals made with optical and microwave sensors into a blended snow cover map.

Climatic information on the snow cover occurrence has been derived from NOAA weekly interactive snow and ice charts produced during the time period from 1972 to 1998. This is so far the longest time period when the spatial resolution of the maps remained unchanged. The spatial resolution of NOAA weekly snow charts generated during that time was about 180 km. From 1998 to 2004 the IMS snow charts were produced daily at about 24 km resolution, whereas in 2004 the spatial resolution was increased to 4 km (**Helfrich, 2007**). Therefore the whole 40+ year long time series of NOAA Interactive snow product cannot be considered homogeneous.

Weekly NOAA snow charts over the 26-years long time period (1972-1998) have been regridded to 30 km latitude-longitude grids and the frequency of occurrence of snow cover for each week was calculated. . Every grid cell of each weekly map was then assigned one of three categories named “snow unlikely”, “snow possible” (or “intermittent snow”) and “persistent snow” depending on the frequency of occurrence of the snow cover in that particular grid cell and in its close proximity. The grid cell was labeled as “snow possible” if on the current, preceding or subsequent week the estimated snow cover frequency of occurrence in any of the grid cells within the 200 km radius from the current grid cell ranged from 1% to 99%. All remaining grid cells with the frequency of occurrence of 0% or 100% were labeled correspondingly as “snow unlikely” and “persistent snow”. Figure 4.5 presents an example of a weekly map of snow cover frequency of occurrence and a

corresponding map of snow cover probability classes (“persistent snow”, “snow possible” and



“snow unlikely”). Since NOAA snow and ice charts are produced only over the Northern Hemisphere, the derived snow cover occurrence statistics is available only south of the equator.

Figure 4.5 – Snow frequency of occurrence (left) and snow cover probability (right) for week 5 of the year derived from NOAA weekly snow cover charts for 1972-1998.

4.3 GMASI Snow and Ice Cover Mapping Algorithms

This section presents the description algorithms incorporated in and used by the GMASI system. Algorithms to derive information on the snow and ice cover from individual satellite sensor data in the visible/infrared and in the microwave spectral range are reviewed first in sections 4.3.1-4.3.4. Next we present the technique combining information on snow and ice derived from different sensors data (section 4.3.5) and the recurrent gap-filling technique used to achieve the spatial continuity in the derived snow and ice maps (section 4.3.6). Finally, section 4.3.7. discusses regional specifics of the snow and ice algorithms implementation.

4.3.1 Snow and ice mapping with METOP AVHRR

The pre-processing function is to ingest the required input data and prepare it for main processing. METOP AVHRR Level 1b swath data are acquired in McIDAS AREA format through McIDAS system from FRAC data set on PLR server (IP: 140.90.213.159). Built in McIDAS routines are used to calibrate and navigate the data. . The output of the preprocessing stage consists of AVHRR swath data files in binary format with observations in every pixel navigated and calibrated. Observations in channels 1, 2 and 3a are calibrated in percent reflectance whereas observations in channels 3b, 4 and 5 are calibrated in brightness temperature. The sensor data are complemented with data on four angles, satellite view angle, satellite view azimuth, solar zenith angle and solar azimuth that completely define the viewing and illumination geometry of each observation. The preprocessed data are saved in separate files for each spectral band and for each geometrical parameter.

The implemented snow identification and mapping algorithm for METOP AVHRR involves two stages, the spectral classification and spatial filtering. A description of these stages is given below.

Spectral classification over land

Spectral classification of the AVHRR imagery is performed only for land pixels. All pixels with the water fraction of 50% or more are considered as “water” and are excluded from further image classification. The fraction of water within each 2 km pixel is calculated using UMD land cover types

map at 1 km resolution. The observed reflectance is normalized to the solar zenith angle and converted to percent values.

The developed snow identification algorithm generally follows the line of snow detection algorithms developed earlier for MODIS, AVHRR, MSG SEVIRI, and GOES Imager instrument data (e.g., Hall et al, 2002, Baum and Trepte, 199, Romanov et al, 1999). It relies on the calculated value of the Normalized Difference Snow Index (**NDSI**), two Snow Indices expressed as a ratio of reflectances in AVHRR bands 1 and 3a (**SI₁**) and bands 2 and 3a (**SI₂**) along with the observed brightness temperature in band 4 (T_4) and reflectances in bands 1,2 and 3a (**R₁**, **R₂** and **R₃**). High **NDSI**, high **SI₁** values along with relatively low infrared brightness temperature in ch.4, low **SI₂** and low NDVI are the primary indicators of the presence of snow within the instrument field of view. The threshold test incorporating AVHRR ch.1 and ch.2 reflectance primarily means to eliminate dark, shadowed or partially covered with water surfaces that can exhibit high **NDSI** and **SI₁** without any snow on the ground. Snow is particularly difficult to identify in dense boreal forests because of the snow masking by the tree canopy. Snow-covered needle leaf forests can still exhibit larger NDVI of up to 0.2. To properly handle these cases we have included an additional set of tests specifically meant to identify snow in the boreal zone.

The image spectral classification algorithm is a threshold-based decision-tree algorithm which is applied on a pixel-by-pixel basis. Image classification algorithms applied over Northern and Southern Hemisphere are generally similar, but have minor differences. The flowcharts of the image classification algorithm for Northern and Southern Hemispheres are shown in Figure 4.6. At the first step of the classification algorithm all pixels with infrared brightness temperature in AVHRR ch. 4 (T_4) below 255K in Southern Hemisphere and below 230K in Northern Hemisphere are attributed to the “cloud” category. In the Southern Hemisphere temperatures below -17⁰ C are very rarely observed at the surface level and therefore are most often are indicative of the cloud in the instrument field of view. In clear sky conditions the magnitude of the brightness temperature in ch.4 can be used as a rough estimate of the land surface temperature.

At the second stage the observed reflectance values are tested for validity and consistency. Pixel observation is considered invalid and the pixel is classified as “undetermined” if the value of solar-zenith angle-corrected reflectance in any reflective spectral band exceeds 120%. Although the reflectance values above 100% do not have a physical meaning, a strong surface reflectance angular anisotropy (or specular reflectance effects) may cause the angle-corrected reflectance to exceed 100%. The only reflectance consistency test incorporated in the algorithm examines the difference between the observed reflectance in channels 1 and 3a. If the reflectance in ch. 3a is zero and the reflectance in ch.1 is above 20%, the pixel observation data is considered inconsistent and the pixel is flagged as “undetermined”. The primary objective of this test is to exclude observations taken at the sunrise or sunset when ch.3b may be turned on instead of ch. 3a.

The third step incorporates several threshold tests to identify snow covered pixels in the satellite imagery. The spectral parameters used in the image classification include AVHRR ch.1, 2 and 3a reflectance (**R₁**, **R₂**, **R₃**), ch.4 brightness temperature (T_4), two snow indices (**SI₁** and **SI₂**) Normalized Difference Snow Index, **NDSI** and Normalized Difference Vegetation Index, **NDVI**. All pixels with the METOP AVHRR ch.4 brightness temperature below 290K are tested for the presence of snow, however for “cold” pixels with the temperature below 273K a special (second) set of somewhat “relaxed” **NDVI** criteria is used. Lastly in the Northern Hemisphere an additional,

third snow test is applied with even further relaxed NDVI threshold value but tighter thresholds for the visible and shortwave infrared reflectance.

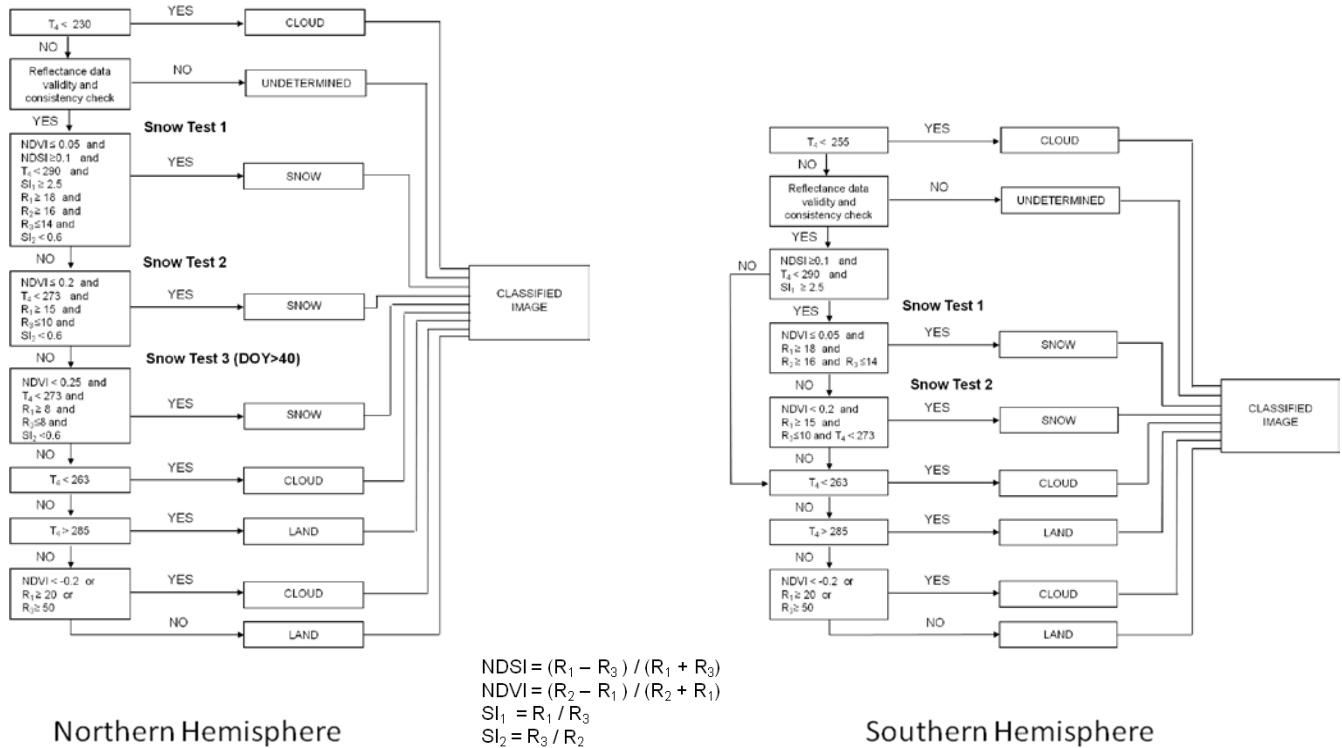


Figure 4.6 – Flow chart of the AVHRR spectral-based image classification algorithm over land. Left: Northern Hemisphere, Right: Southern Hemisphere. Threshold values are given in degrees K for the brightness temperature and in percent for the reflectance

Pixels that were not identified as “snow” are separated into snow-free land (or “land”) and “cloud” categories at the next stage. First a very rough infrared brightness temperature test is applied where “cold” pixels with $T_4 < 263K$ are labeled as “cloud” and pixels with $T_4 > 285K$ are labeled as “land”. The remaining pixels are separated into “land” and “cloud” by their reflectance value in ch.1 and 3 and their **NDVI** (see Fig. 4.6).

The threshold values for all tests were determined empirically using a simple trial and error approach. The accuracy of the image classification was also assessed qualitatively by visual comparison of classified and original false-color composited images.

Image spectral classification over ocean

Within the GMASI system ice cover with AVHRR data is identified only in the Northern Hemisphere. Although microwave observations are much more effective in detecting and mapping ice cover, coarse, about 30 km spatial resolution of these measurements prevent from efficient ice mapping on mid and high-latitude lakes and smaller water reservoirs. AVHRR-based ice retrievals are applied to complement microwave retrievals along the ice cover boundary in the open ocean and are used as a sole source of information on the ice cover over midlatitude lakes. In the Southern Hemisphere except of several small lakes in Patagonia ice cover is found only in the Southern Ocean where application of coarser resolution microwave observations for mapping ice extent is sufficient.

Similarly to the snow detection algorithm, the algorithm to identify ice over water bodies implements a threshold-based decision-tree approach. The pixels is labeled as ice-covered if the following conditions are met: $SI_1 > 6$, $T_4 < 274$ K, $R_1 > 15$, $R_3 < 1.2$, $-0.3 < NDVI < 0$. An additional threshold test of $R_2 < 10$ is applied to distinguish broken/thin ice from thick continuous ice cover. Pixels with the brightness temperature above 285K are labeled as “water”. Pixels than were not identified as “ice” but have brightness temperature in band 4 below 260 are labeled as “cloudy”. Clouds in remaining pixels with the skin temperature within 260 to 285K are identified with two tests, $R_1 > 15$, or $R_3 > 10$. All other pixels are labeled as “clear water”.

Spatial filtering

The developed classification algorithm based on spectral threshold tests properly discriminates snow from snow-free land surface and from clouds in most cases, but not always. Errors in snow identification and mapping primarily occur due to confusion of snow with clouds which exhibit spectral features similar to snow. Some mixed land-cloud scenes can also produce a spectral response similar to snow and thus may also be erroneously classified as snow. To identify and eliminate these spurious snow retrievals we have developed and implemented a number of additional tests based on available information on the land surface properties or on spatial consistency criteria. The developed tests include (1) Temperature climatology test, (2) Isolated snow pixel test, (3) Temperature spatial homogeneity test, (4) Snow small cluster filter and (5) Cloud neighbor filter. All tests are applied only to pixels classified as “snow” by the spectral-based algorithm. Pixels that pass through all these tests are flagged as “confirmed snow”. All “potential snow” pixels that fail at least one test are labeled as “cloudy”. Details of all filters are given below.

(1) Temperature Climatology Test

Within this test the pixel IR brightness temperature value observed in AVHRR ch.4 (T4) is compared with the multiyear mean (climate) value of the land surface temperature (LST) for the pixel location for given time of the year. The climatic LST is corrected for the elevation of the pixel assuming a 7 degC/km vertical temperature gradient. If the observed T4 is over 20K below the climatic LST, “snow” is rejected and the pixel is labeled as cloudy. The test uses monthly LST climatology developed as part of the ISCCP project. To estimate the climatic LST value for the given day a linear interpolation is performed between LST values for the two consecutive months. When performing interpolation monthly climatic LST values are assumed valid for the 15th day of the month.

(2) Isolated Snow Pixel Test

Misclassifications of clouds as snow most often appear as isolated “snow” pixels in the midst of clouds. To eliminate these misclassifications a 3x3 pixel sliding window is used to locate isolated

“snow” pixels completely surrounded by cloudy pixels. If all eight pixels next to the “snow” pixel in the 3x3 box are cloudy, the “snow” pixel is rejected and is labeled as cloudy.

(3) Temperature Spatial Homogeneity Test

The idea of this test is to check whether there are any pixels in the neighborhood of the "snow" pixel that are much warmer than the "snow" pixel. Outside of mountainous areas and large water bodies the spatial gradient of the land surface temperature is limited. Therefore a substantial number of much warmer pixels may indicate that identification of "snow" is erroneous. For this test a sliding window of ~100x100 km (51 x 51 grid cells) centered at the “snow” pixels is applied. Within this region we identify the pixels whose IR brightness temperature in AVHRR ch. 4 exceeds T₄ of the “snow” pixel by more than 20K. The “snow” pixel is reassigned to the “cloud” category if the number of these much warmer pixels found within the sliding window area exceeds 10 (or more than 0.4%). The test is not applied in high altitude areas with elevation above 900 m. It also does not account for the temperature of pixels covered by water for more than 30% or located more than 300m below the central "snow" pixel.

(4) Snow small cluster filter

Sliding window of 10x10 pixels (grid cells) is used to identify isolated small clusters of “potential snow” pixels in the midst of clouds. There is high likelihood that in these pixels clouds were falsely classified as snow. If all pixels on the window perimeter are cloudy and the fraction of clear pixels is less than 15%, pixels previously identified as “snow” are reassigned a “cloudy” flag.

(5) Cloud neighbor filter

A 3x3 sliding window centered on a “snow” pixel is examined. If any other of the pixels within the box is cloudy, the “snow” pixel is labeled as “cloudy”. The test is applied to all snow pixels with surface elevation below 500m. The surface elevation condition is added to retain capability to properly identify snow caps on mountains.

As of October 2013 all consistency tests in the AVHRR operational snow mapping algorithm were turned on.

An example of the daily snow cover map generated from METOP AVHRR is shown in Figure 4.7. The derived snow cover distribution is very similar to the snow cover mapped by MODIS.

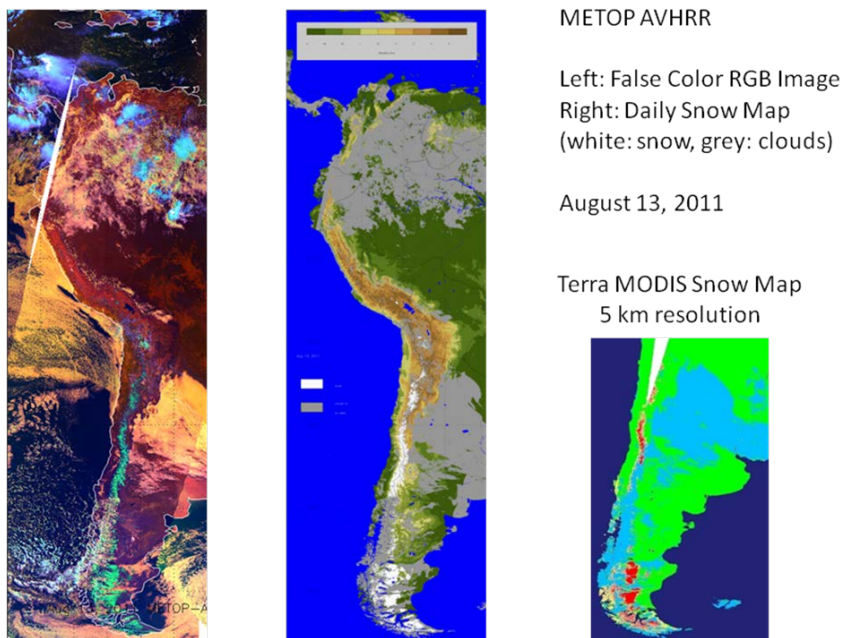


Figure 4.7 – Example of METOP-AVHRR false-color composite image and corresponding snow cover map over South America. Corresponding MODIS snow map at 5 km resolution is shown in the right.

AVHRR Snow /Ice Mapping Algorithm Output

To save the processing time METOP AVHRR image classification and snow identification is performed only over selected regions in the Northern and Southern Hemisphere where seasonal variations of the snow cover are expected. In the Northern Hemisphere snow cover is mapped everywhere in North America (including Greenland), Eurasia north of 25° N and in Africa north of 25°N. In the Southern Hemisphere areas where snow cover is mapped include the Western part of South America, the Southern part of Africa and South-East Australia and New Zealand. At this time the Antarctic continent is assumed permanently snow covered and snow cover is not identified and mapped in this region. The rest of the globe is assumed snow free all year round. Ice cover with AVHRR is identified and mapped only in the Northern Hemisphere north of 25°).

Table 4.2 – Coverage and size of METOP AVHRR daily snow/ice regional maps

Region	Latitude range	Longitude range	Dimension (columns, lines)	Parameters derived
Eurasia	25°N - 90° N	25°W - 0 - 165°W	5500, 1625	Snow, Ice
North America	25°N - 90° N	20°W – 180°W	4000, 1625	Snow, Ice
South America	20°N - 56°S	60°W – 84°W	600, 1900	Snow
Australia & New Zealand	25°S – 49°S	140°E – 180°E	1000, 600	Snow
Southern Africa	24°S – 36°S	13°E – 37°E	600, 300	Snow

The output of the AVHRR-based snow mapping system includes separate daily snow cover maps over three regions in Southern Hemisphere, specified above along with North America and Eurasia. Table 4.2 presents the size and the coverage of all individual regional snow and ice maps. All snow and ice maps are generated on a latitude-longitude grid with 0.04 deg (or about 4km at the Equator) grid cell size. Every land pixel in the gridded map is attributed to one of four categories: snow cover, snow-free land, cloud, undetermined/no retrievals/no data. If ice is derived, “water” grid cells of the map are classified into “ice-free water”, “ice cover”, cloud” or “undetermined/no data” categories. Examples of all regional AVHRR-based snow /ice products are shown in Figure 4.8

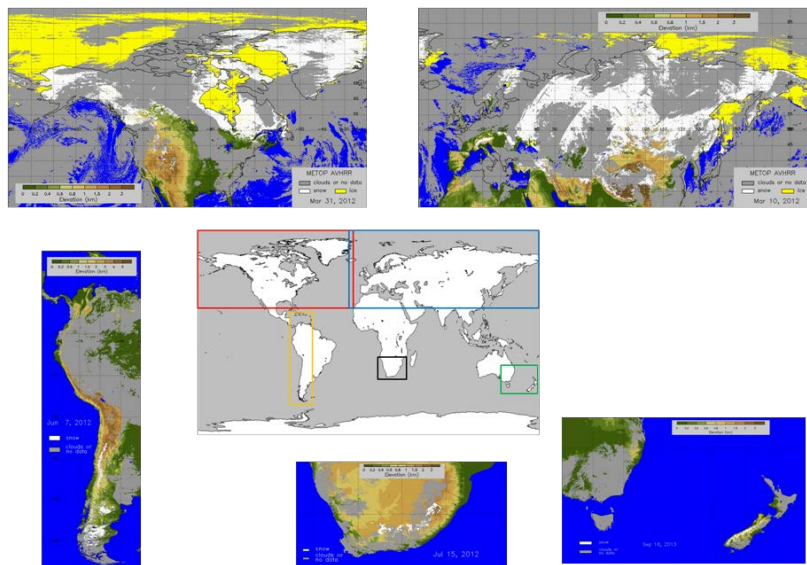


Figure 4.8 – Coverage and examples of regional AVHRR-based snow/ice maps

At this time only daily maps are produced. Development of weekly and/or monthly snow cover statistics is assumed in the potential future enhancement of the system.

4.3.2 Snow and ice cover mapping with GOES Imager data

Algorithm

GOES Imager instrument lacks observations in the shortwave infrared spectral band at 1.6 μm . Therefore to identify snow cover observations in the middle infrared at 3.9 μm have to be used. The scene reflectance at 3.9 μm wavelength is derived from the observed brightness temperatures in the middle infrared and in the far infrared (centered at 11.5 μm) spectral bands following the approach of Allen et al (?).

Repeated observations from GOES Imager during the day are used in the snow mapping algorithm in two ways. First, all daytime images are composited and for every grid cell observation with the maximum infrared brightness temperature is retained. This compositing procedure allows for reducing the number of cloud-contaminated grid cells in the map and thus improve the area coverage. Second, Temporal variations of the scene visible reflectance and infrared brightness temperature are utilized to better discriminate snow cover from clouds that exhibit a spectral response similar to snow. A detailed description of the algorithm is provided in Romanov et al., 2000 and Romanov et al., 2003.

The algorithm to identify ice in the GOES Imager field of view has much in common with the snow identification algorithm.

GOES Imager snow/ice mapping algorithm output

The output product of the GOES Imager snow and ice mapping algorithm presents a binary map of snow and ice cover distribution where every grid cell is attributed to one of six categories: “snow cover”, “snow-free land”, “ice-free water”, “ice on water” “cloud” and “undetermined/no data”. Daily maps of snow and ice cover distribution are generated on a latitude-longitude grid with 0.04 degree grid cell size (or about 4 km spatial resolution). The domain of the maps incorporates the North America mid-latitude region (see Table 4.3) . Snow and ice mapping east of 100⁰W is performed with GOES East data whereas the west of 100⁰W snow and ice maps are generated with GOES-West data. An example of the GOES-based snow and ice map is given in Figure 4.9

Table 4.3 – Coverage and size of GOES-based daily snow/ice map

Region	Latitude range	Longitude range	Dimension (columns, lines)	Parameters derived
North America	25 ⁰ N - 66 ⁰ N	50 ⁰ W – 170 ⁰ W	3000, 1025	Snow, Ice

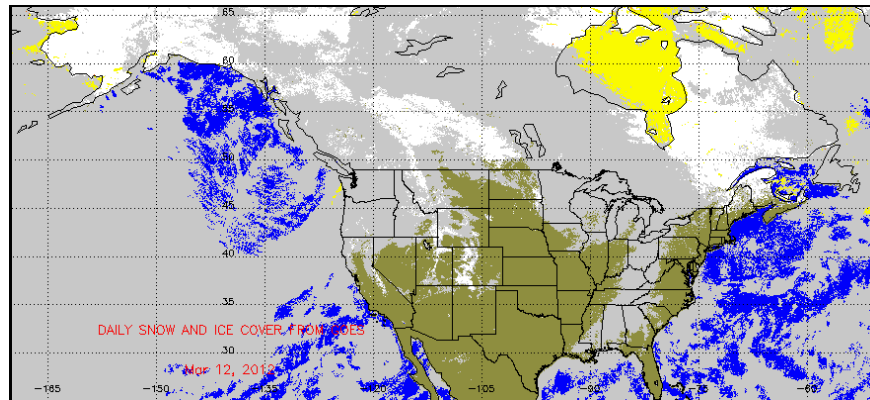


Figure 4.9 – Example of GOES-Imager-based daily snow/ice map. Snow is shown in white, clouds are in gray and ice is in yellow.

4.3.3 Snow cover mapping with METEOSAT SEVIRI

The spatial domain of Meteosat SEVIRI does not include large sea areas or a large number of inland water bodies affected by seasonal ice, therefore only snow cover is identified and mapped with the SEVIRI instrument data. The algorithm generally follows the logic of the snow mapping algorithm developed for GOES Imager, but instead of the middle infrared spectral band observations in the shortwave infrared are used. The algorithm also makes use of observations in the near-infrared spectral band.

The developed technique for snow cover identification uses SEVIRI observations in the visible (channel 1, centred at 0.6 μm), near-infrared (channel 2 centred at 0.8 μm), shortwave infrared (channel 3, centred at 1.6 μm) and infrared (channel 9, centred at 10.8 μm) spectral bands. Since clouds are generally opaque in the visible, mid-infrared and infrared spectral bands, the retrievals are limited to cloud-clear scenes. A complete data processing scheme to derive maps of snow fraction involves data preprocessing, data compositing, spectral classification and consistency testing.

At the preprocessing stage SEVIRI images acquired every 30 minutes are registered to a latitude-longitude projection with a 0.040 by 0.040 degree grid size, or approximately 4km spatial resolution.

Satellite observations are processed over the area extending from 25 N to 66 N and from 25 W to 55 E. Extending the area further north and east is not feasible because of large satellite view zenith angles. Daytime SEVIRI images acquired during a day are then composited and observations with maximum infrared brightness temperature are retained in every map grid cell. Since the “warmest” observation is most often the least cloud-contaminated, this procedure provides an effective cloud-clearing of the composited image.

Both the daily composited image and all individual 30-minute instantaneous images acquired during a day are further utilized in the snow identification procedure. This procedure uses both spectral signatures and temporal stability criteria to ensure the most accurate image classification and snow mapping. The daily composited image is subjected to a threshold-based decision-tree unsupervised spectral-based classification, which separates the image pixels into “snow”, “snow free land surface” and “cloud” categories. Besides the brightness temperature in SEVIRI channel 9 (T9),

visible and shortwave-infrared reflectance (R1 and R3 respectively) the classification algorithm utilizes a “snow index” (SI, defined as the ratio $R1/R3$). The idea of using the ratio of the visible to the middle-infrared or short-wave infrared reflectance to identify snow in satellite images was put forward about two decades ago (see Bunting and d'Entremont [1982]). Due to a low reflectance of the snow cover in the middle infrared and a high reflectance in the visible, the snow index enhances the difference of the spectral response of the snow cover from the response of other surfaces and is thus beneficial for snow detection.

The sequence of spectral tests included in the snow identification algorithm is shown in Figure 2.

Fixed threshold values were used for SI (SIT=1.2) and T9 (T9T=2900 K), whereas for the visible and shortwave infrared reflectance, the threshold values (R1T and R3T) were assumed to be location dependent and were defined for every grid cell of the map. To establish R1T and R3T and the model approximating the land surface reflectance anisotropy in the visible and in the shortwave infrared we have used statistics of MSG cloud-clear observations accumulated during snow-free periods of the first half of the year 2005. Values of R1T and R3T for a grid cell were set equal to values exceeding the average visible and shortwave infrared reflectance for this grid cell by twice the standard deviation. The land surface reflectance anisotropy was characterized using a semi-empirical kernel-driven model of Roujean et al. (1992). The model is governed by two coefficients, which are the loadings on the kernels representing correspondingly volumetric scattering and surface geometrical effects, and a constant.

After snow-covered pixels are separated, the image classification procedure continues with discriminating non-snow pixels into “clouds” and “snow free land surface”. Observations having a low (below 265 K) brightness temperature or a moderate brightness temperature (within 265K to 285K) along with a high visible reflectance, high shortwave infrared reflectance and low normalized difference vegetation index ($NDVI=(R2-R1)/(R2+R1)$) are labeled as “cloudy”. All remaining image pixels are assigned a “snow free land surface” flag.

Experience with numerous MSG SEVIRI scenes has shown that some clouds exhibit spectral features similar to snow and thus cannot be distinguished from snow cover only from instantaneous spectral measurements. To resolve this ambiguity, we complemented the image classification algorithm with a temporal stability test (see Fig.1). In this test an intra-day temporal variability of the scene temperature and reflectance is employed as a predictor to distinguish between cloudy and cloud clear pixels. The test is applied only to those image pixels, which were classified as “snow covered” according to their spectral response. For every “snow covered” pixel, the “warmest” observation retained in the daily composite is compared to all observations over this location acquired during the day. The pixel is confirmed as “snow”, if three or more instantaneous observations are found, which are spectrally similar to the “warmest” one. Observations are considered similar if corresponding values of R1 and T9 are within 5% and 8 K, respectively.

These threshold values were determined empirically through a visual examination of satellite imagery and quantitative analysis of daily time series of satellite observations over selected targets representing different surface types. It should be noted that the values of thresholds given above are very close to corresponding threshold values proposed by Key and Barry [1989] to detect clouds over snow covered land surface in the polar area from a series of daily NOAA AVHRR images.

In order to further improve the removal of falsely identified snow cover we applied two additional tests based on the land surface temperature climatology and the snow cover climatology. Snow identified in the satellite imagery is rejected if (1) the scene infrared brightness temperature is more than 20K below its climatic value for the given location and the time of the year or (2) within the area of 20 by 20 grid cell (or about 80 x 80 km) centered at the pixel location snow cover has never been observed on the given week of the year as well as on two adjacent weeks. The land surface temperature monthly climatology was adopted from the International Satellite Cloud Climatology Project (ISCCP), whereas the snow cover statistics was calculated from NOAA weekly snow cover charts for the period from 1972 to 2004.

Comparison with in situ station reports has shown that snow identified with Meteosat SEVIRI is confirmed by ground-based stations in over 95% of cases.

Meteosat SEVIRI snow mapping algorithm output

The output product of the Meteosat SEVIRI snow mapping algorithm presents a binary map of snow cover distribution where every land grid cell is attributed to one of four categories: “snow cover”, “snow-free land”, “cloud” and “undetermined/no data”. Daily maps of snow cover distribution are generated on a latitude-longitude grid with 0.04 degree grid cell size (or about 4 km spatial resolution) covering Europe up to 66°N, Middle-East Asia and northern Africa (see Table 4.4). Figure 4.10 presents an example of daily snow map generated with MSG SEVIRI data.

Table 4.4 – Coverage and size of MSG SEVIRI-based daily snow/ice map

Region	Latitude range	Longitude range	Dimension (columns, lines)	Parameters derived
Europe & N.Africa	25°N - 66° N	25°W – 55°E	2000, 1025	Snow, Ice

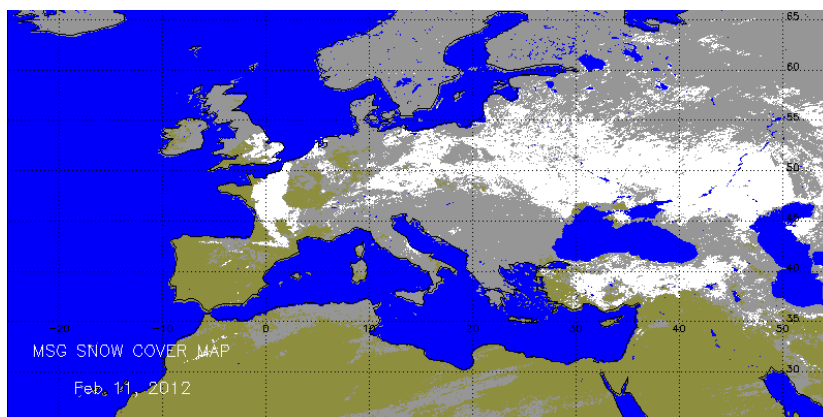


Figure 4.10 – Example of MSG SEVIRI-based daily snow map. Snow is shown in white, clouds are in gray.

4.3.4 Snow and ice mapping using DMSP SSMIS data

Identification of both snow and ice cover with SSMIS data is performed through a series of threshold tests. The tests incorporate the SSMIS-observed brightness temperature values as well as spectral and polarization indices. In some cases SSMIS observations do not allow for a reliable attribution of a scene to a particular category (“ice”, “ice-free water”, “snow cover” or “snow-free land surface”). Therefore additional temporal and spatial consistency tests are applied to identify and eliminate questionable retrieval results. Both algorithms (snow and ice) utilize daily observations from all available SSMIS sensors both at the ascending and descending nodes. Repeated observations available from multiple DMSP satellites allow for most reliable and accurate snow and ice cover mapping.

Preprocessing of DMSP SSMIS data includes unpacking the level1b global swath data files, navigating and gridding the data. The spatial resolution of SSMIS spectral bands used for ice identification is different and ranges from 27.5 km for 37GHz bands to 44.8 km for 19 and 22 GHz bands. As a common geographical projection for all bands we have selected a lat-lon projection at 1/3 degree (or about 30 km) grid cell size. This projection has been historically used at NOAA NESDIS for environmental data products from SSMIS and older SSMI sensor data.

Within the developed preprocessing algorithm individual gridded brightness temperature datasets are generated for each satellite at each node (ascending and descending). With three currently operational DMSP satellites carrying SSMIS instruments (F-16, F-17 and F-18) six global daily brightness temperature datasets are produced.

DMSP SSMIS Snow Mapping Algorithm

An important advantage of SSMI is availability of observations from multiple satellites. Since the end of the 1990s, SSMI and, later, SSMIS observations were conducted from three or more satellite platforms at the same time yielding from 4 to 6 daily “looks” in mid- and high latitude regions. Information on the temporal variation of the scene response provided by multiple daily observations in the microwave helps to better distinguish snow cover from precipitating clouds which may exhibit a spectral response in the microwave similar to snow.

Snow cover in the SSMIS imagery is identified and mapped using the algorithm of Grody (Grody and Basist, 1996). The algorithm utilizes observations of the brightness temperature at 22, 37 and 85 GHz frequency at vertical polarization and at 19 GHz at both vertical and horizontal polarization. Snow cover is identified through application of a series of threshold-based tests which incorporate the brightness temperature values in individual spectral bands, along with the spectral and polarization difference of brightness temperatures in a number of spectral bands. The algorithm specifically focuses on discrimination of snow cover from other natural scenes that may produce a spectral response in the microwave similar to snow, particularly precipitating clouds, cold deserts and frozen soil. A special test is applied to properly identify glacialized snow cover inherent to Greenland and Antarctica.

The original algorithm of Grody has been developed and tested with observations of SSMI. Spectral imaging bands of SSMIS do not exactly match the corresponding bands of SSMI. To adjust the

brightness temperatures observed with SSMIS to fit the SSMI data the algorithm of Yan and Weng, (2008) is applied.

Multiple daily observations from SSMIS are used in NOAA GMASI which identifies snow in all six daily overpasses of three DMSP satellites. To eliminate the effect of possible instrument noise and occasional errors due to atmospheric effects only snow cover identified in a give grid cell three or more times during the day is considered “confirmed snow” and is further used in merging with optical snow retrievals. An example of a daily map of the number of positive snow identifications (or “snow hits”) with the data of SSMIS sensors onboard three DMSP satellites is given in Fig. 4.11.

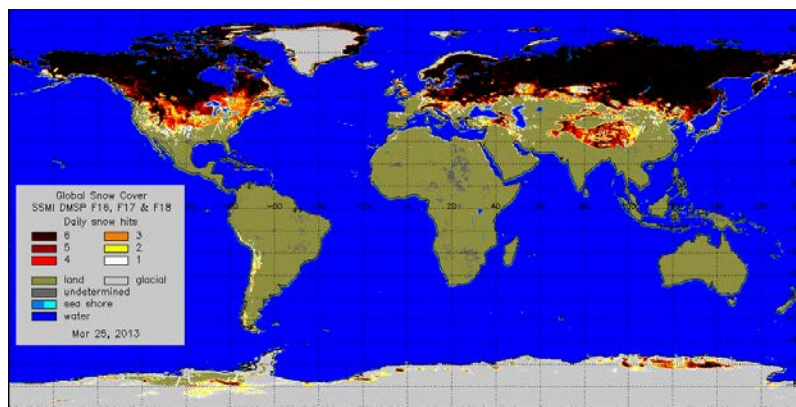


Figure 4.11 – Map of the number of positive snow identifications (or “snow hits”) from the data of SSMIS sensors onboard three DMSP satellites

DMSP SSMIS Ice Identification Algorithm

The implemented ice identification and mapping algorithm for DMSP SSMIS involves four stages, the image compositing, the spectral classification, temporal consistency testing, spatial filtering and blending. A description of these stages is given below.

Image Compositing

Because of a narrow swath width of SSMIS instrument, daily observations from one satellite leave gaps between neighboring swaths and therefore do not completely fill in all grid cells in the gridded 1/3 degree spatial resolution global map. To achieve a complete daily coverage of the globe with microwave observations SSMIS data from all available DMSP satellites at each node are composited. Since there is no indication of a better performance of any of the currently operational SSMIS sensors, the compositing is performed first, by the node (starting with the descending node and followed by ascending node) and, second, by the satellite number (starting with F-16 and ending with F-18). Within the compositing procedure the grid cell in the composited map is updated if hadn't have an associated prior valid SSMIS observation or if the spectral gradient of the brightness temperature in 19GHz and 37GHz spectral bands at vertical polarization ($T_{17V}-T_{37V}$) observed in the current image exceeds the composited value. Ice-covered scenes typically exhibit a larger $T_{19V} - T_{37V}$ spectral gradient than the ice-free scenes, therefore compositing of the imagery

by retaining observations with the largest brightness temperature spectral gradient helps to reduce the “loss” of the ice cover at the further steps of the ice identification and mapping algorithm.

Spectral identification of the ice cover

The ice spectral identification algorithm follows the NASA Team ice identification algorithm by utilizing two major indices, the polarization ratio at 19 GHz:

$$PR_{19V}=(T_{19V}-T_{19H})/(T_{19V}+T_{19H})*100$$

and **19V/37V** spectral gradient:

$$GR_{37V19V}=(T_{37V}-T_{19V})/(T_{37V}+T_{19V})*100,$$

where T_{37V} , T_{19V} and T_{19H} are, correspondingly the observed brightness temperature in the 37GHz band at vertical polarization, in the 19GHz band at vertical polarization and in the 19GHz band at horizontal polarization.

The two spectral tests are applied to the daily gridded brightness temperature values. The grid cell is labeled as “potential ice” if $PR_{19V} \geq 15$ and $GR_{37V19V} \leq 7$. Otherwise the pixel is labeled as “no ice”. Prior to applying the spectral ice test, all brightness temperature values are tested for their validity. Observations with brightness temperature value in any band below 80K or exceeding 320K is considered invalid. An additional test incorporating the difference of brightness temperature values in SSMIS 19GHz and 22GHz bands at vertical polarization ($T_{22V}-T_{19V} < 20$) is applied to identify and eliminate physically invalid observations.

Temporal consistency testing

The temporal consistency test is applied to pixels identified as “potential ice” by the spectral classification algorithm. The test compares the daily composited brightness temperature values in the “potential ice” pixels with temperature values in corresponding grid cells observed by each satellite at each node to calculate the number of daily SSMIS observations that were spectrally similar to the one in the composited image. Observations are considered spectrally similar if the difference of corresponding brightness temperature values in all of SSMIS bands remains within 5K. A “no ice” test is also applied to each grid cell of each satellite’s image at the ascending and descending node. A pixel is classified as ‘no ice’ (meaning “water or “undetermined”) if $PR_{19V} \geq 18$ or $GR_{37V19V} \geq 8$ or $T_{22V}-T_{19V} > 20$.

The “potential ice” grid cell passes the temporal consistency test if during the day at least one observation was found that was spectrally similar to the observation retained in the composited image and if there were no observations in the grid cell classified as “no ice” during the day.

Spatial filtering

Spatial filters are applied to fill in at least some gaps in the current day ice map and to eliminate potentially erroneous ice/water retrievals. Separate tests are applied to grid cells located in the vicinity of the shore line (next to “land” grid cells) and to grid cells located in the open sea. The land-water mask used with SSMIS data is generated by aggregating 1 km resolution USGS

GTOPO30 land/water mask data within at 1/3 degree grid cells. Depending upon the fraction of land and water within the 1/3 degree grid cell or its proximity to the shore line every grid cell attributed to one of five categories (Open Water, Far Shore, Near Shore, Shore and Land).

In the open sea the spatial filter identifies isolated “water”, “ice” or “undetermined” grid cells by examining 3x3 grid cell boxes. These grid cells are relabeled to match the category of the surrounding grid cells.

Mixed land/water scenes may sometimes generate a spectral response in the microwave similar to ice resulting in false ice identification along the shore line (sometimes called a “land spillover” effect”). Eliminating these false ice identifications is the major objective of the spatial filter applied to grid cell in the coastal zone. Within this test for every grid cell in the coastal zone identified as “ice” we check the status of bordering grid cells. The “ice” identification is confirmed if no “open water” is found in the bordering grid cells.

DMSP SSMIS snow and ice mapping algorithm output

The output of DMSP SSMIS algorithm incorporates two maps characterizing the global distribution of snow and ice cover. Snow cover is characterized in terms of the number of positive snow identifications during the day (see example in Figure 4.11). Daily ice cover map presents the ice cover distribution (Figure 4.12). Both maps are generated on a latitude-longitude grid with 1/3 of a degree (or about 30 km) grid cell size Some grid cells in both daily maps may not be reliably classified and thus are labeled as “undetermined”.

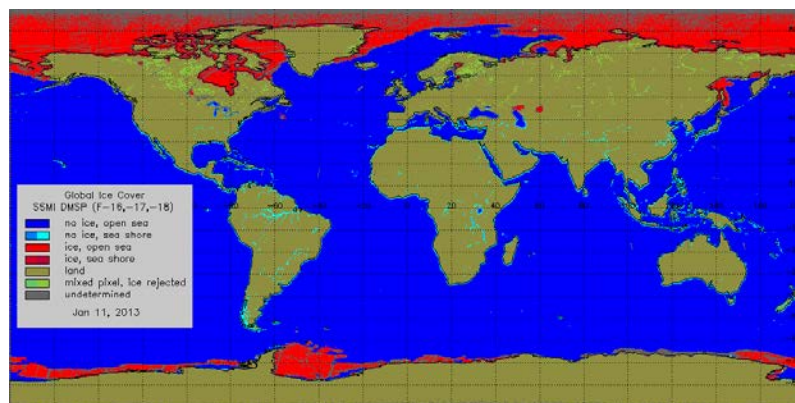


Figure 4.12 – Daily global ice map derived from SSMIS DMSP data

4.3.5. Combining snow/ice retrievals from different sensors data

Once daily data from all satellite sensors are processed, snow and ice daily maps from individual sensors data are combined to generate a blended continuous snow and ice map.

Generation of the combined snow and ice cover map involves two steps. First, information on snow and ice derived from METOP AVHRR is complemented with snow and ice identified from geostationary satellite data. At the second step snow and ice maps derived from satellite observations in the visible and infrared from both polar-orbiting and geostationary satellites are complemented with snow and ice information inferred from satellite observations in the microwave.

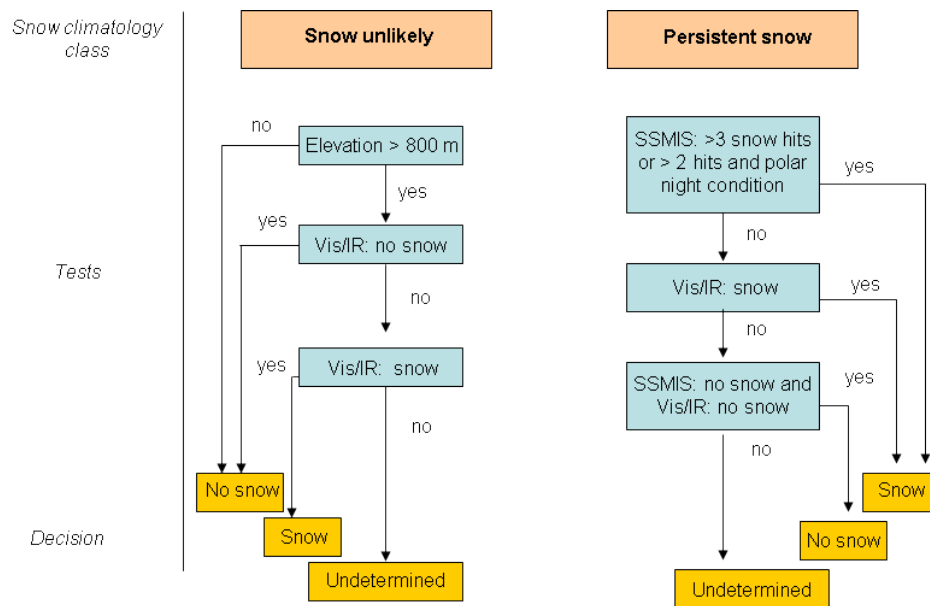
All snow/ice maps based on the data from satellite sensors operating in the visible and infrared are produced on the same, 4 km spatial resolution latitude-longitude grid. This identity of the grids facilitates merging individual snow and ice products. When combining maps derived from METOP AVHRR and from geostationary satellites sensors, the preference is given to the polar orbiting satellite product due to the wider area coverage of polar orbiting satellite data, higher spatial resolution of AVHRR observations and better navigation accuracy. Therefore the combined visible/infrared daily snow/ice cover map is first filled in with the METOP AVHRR clear sky retrievals and then grid cells identified as “cloudy” or undetermined by METOP AVHRR are filled in with available clear sky retrievals from GOES and MSG.

Although snow and ice retrievals from geostationary satellites may help better and timely identification of changes in the snow/ice cover extent and distribution in certain cases, availability of this data is not critical for the overall system operation. The use of GOES Imager data is further complicated by fast degradation of visible sensors of GOES Imager instrument requiring their frequent calibration updates and by substantial image co-registration errors. To easily include or exclude geostationary satellite snow/ice retrievals from the data processing stream a switch has been incorporated in the system. In 2014 it was determined that efforts needed to maintain a multiplatform system configuration involving data from geostationary satellites are not adequate to the benefits of having additional snow and ice retrievals from sensors onboard Meteosat and GOES. Therefore visible and infrared observations only from AVHRR onboard METOP satellite are used in GMASI.

The general approach to combining snow observations in the visible/infrared and in the microwave within the system is based on three basic principles. First, it uses a well established fact that snow retrievals in the visible and infrared are more accurate and reliable than retrievals with microwave data. Therefore almost always when satellite retrievals in the visible and infrared are available (i.e., are not cloudy or undetermined due to the lack of daylight) they are used to fill in corresponding grid cells in the combined daily snow map. Second, because of known physical limitations of snow remote sensing in the microwave, a cautious approach is adopted with respect to the use of microwave retrievals when snow observations in the visible and infrared are not available for any reason. In particular, because of frequent misses of the snow cover in microwave products (partially due to inability to detect melting and shallow snow cover), all “no snow” identifications by the SSMIS-based snow map is considered unreliable and are not used in the blended snow map. Due to inability to properly discriminate snow cover from cold rocky surfaces in the microwave spectral range, spurious snow cover frequently occurs in microwave snow products in mountainous regions. To prevent these errors from propagating into the combined map, microwave snow retrievals in elevated areas are mostly disregarded and are not incorporated in the blending algorithm. Third, the snow cover climatology is accounted for in the algorithm. A more cautious approach to the use of snow cover mapped in both products, visible/infrared and microwave is applied in the areas with lower probability of the snow cover occurrence. To allow for an easy combining and merging of snow and ice retrievals from observations in the visible/infrared and in

the microwave spectral bands, microwave snow and ice products are regrided by replication to the 4 km latitude-longitude grids of snow and ice products based on observations in the visible and infrared.

The decision making process within the snow blending algorithm depends on the probability of snow cover occurrence in the particular location on the given time of the year. In the “snow unlikely” region only visible/infrared retrievals are used and snow cover identified only in elevated areas ($h > 880$ m) is incorporated in the blended product (see Figure 4.13). In the “persistent snow” region snow identified by either visible/infrared or microwave instruments is incorporated in the blended map. However in the case of the microwave data snow cover has to be reported at least three times during the day (or at least two times in the polar night conditions) to be considered as confidently identified. The blending algorithm in the “snow possible” regions depends on the topography and the forest cover. Over elevated areas only visible/infrared snow retrievals are used. Over densely forested non-elevated areas snow cover persistently identified in the microwave spectral bands (with four or more positive “snow hits” during the day) may override “no snow” identification in the visible and infrared. The latter clause has been introduced to reduce possible snow misses in the visible and infrared products due to snow masking and shadowing by the vegetation canopy. Outside of these two regions clear sky snow or no snow retrievals in the visible and infrared snow product are complemented by positive snow identifications in the microwave with three “snow hits” or over if visible/infrared retrievals during the day were not available for any reason. If none of the conditions specified above holds, the grid cell in the combined map is left undetermined.



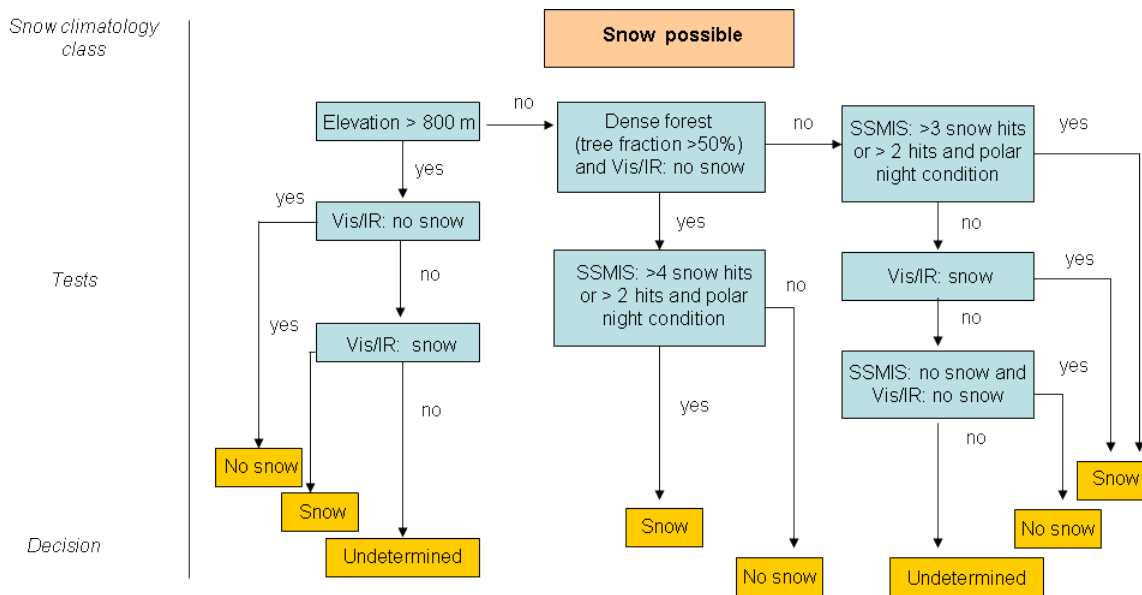


Figure 4.13 – Flow chart of the snow cover blending algorithm for “snow unlikely” and “persistent snow” climatological categories (upper) and for “snow possible” climatological category (lower)

When combining ice retrievals in the visible/infrared and in the microwave, rather than the ice cover climatology, we apply a static map delineating regions where ice cover may exist (see Figure 4.14). Outside of these regions identified ice is rejected. The boundaries of the “ice possible” region were determined from the automated snow and ice maps generated with the Automated Snow and Ice Mapping System during the time period from 2002 to 2011.

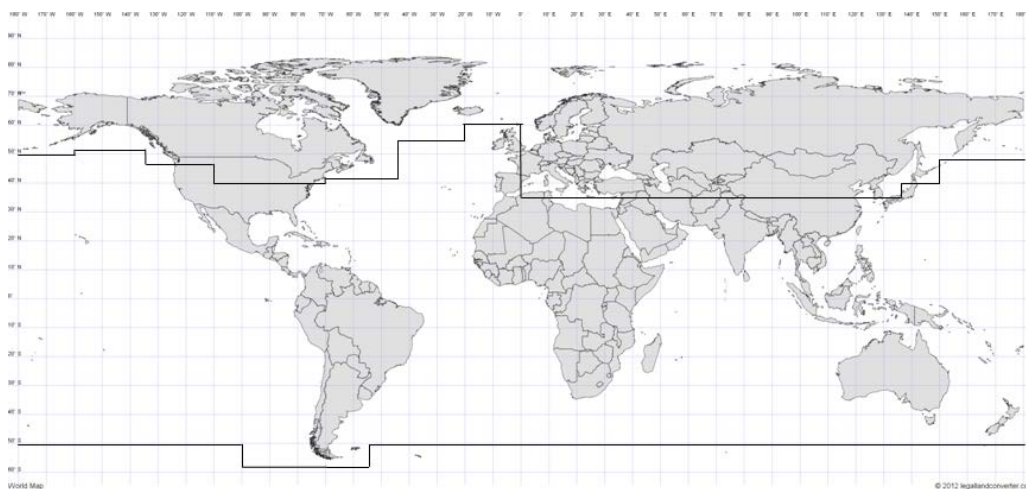


Figure 4.14 – Static boundaries delineating “potential ice” regions. Ice is identified north and south of the two boundaries. Ice is also mapped on lakes in high-elevated areas in the Tibet region.

In contrast to the blending algorithm applied to the snow cover products, when combining ice retrievals the priority is given to the microwave product due to its much better effective area coverage. Ice retrievals in the visible and infrared are used to complement the ice cover product in the microwave primarily along the shore line and in the grid cells adjacent to the areas identified as ice covered by the microwave product. They are also applied over small inland water bodies where the spatial resolution of the microwave data is inadequate and over midlatitude water bodies where frequent mid winter season melt-freeze events may hamper accurate ice cover identification and monitoring from satellite observations in the microwave. Ice retrievals in the visible/infrared are also utilized when there was no reliable estimate of the state of the ice cover from microwave measurements or microwave observations over a given location were not available at al. Details of the blending technique are given in the algorithm flow chart in Figure 4.15.

4.3.6 Recurrent gap-filling algorithm

As it is obvious from the description of the algorithms used to combine snow and ice observations in the visible/infrared and in the microwave, some grid cells of the map may not be updated on the current day due to the lack of valid/reliable retrievals. To achieve the spatial continuity of the daily product a recurrent gap-filling approach is applied. Within this approach grid cells left undetermined after daily snow and ice retrievals have been combined are filled in with the most recent in time reliable earlier snow and ice retrieval results. This latter technique clearly brings in additional inertia to characterization of changes in the snow and ice cover distribution, but provides a gap free coverage of the whole area. Continuous, gap free coverage of the snow and ice maps is an important factor facilitating the use of this product in numerical model applications.

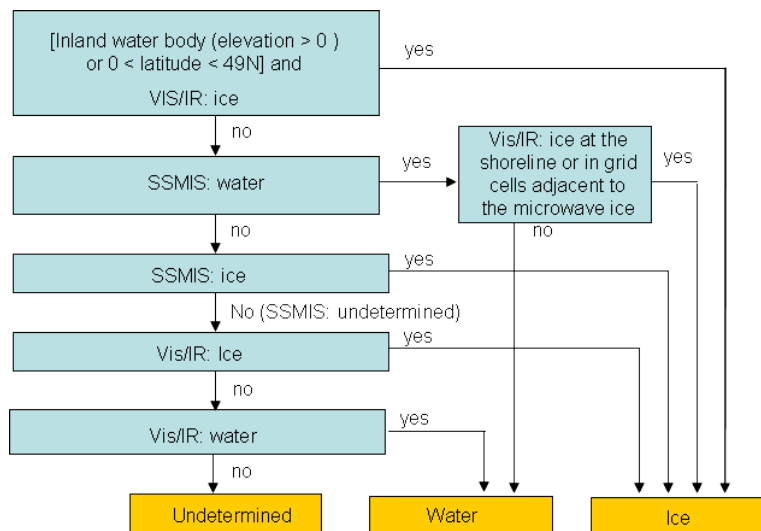


Figure 4.15 – Flow chart of the procedure to combine ice retrievals in the visible/infrared and in the microwave.

4.3.7 Regional specifics of the algorithm implementation

The full set of satellite data listed in section 3.0 is used for mapping snow and ice cover only in the Northern Hemisphere. In the Southern Hemisphere except of Antarctica snow cover is mostly confined to mountainous areas. Outside of the mountainous areas the occurrence seasonal snow cover is rare and if snow occurs, it is most often, patchy, shallow and/or melting. Application of microwave observations to map and monitor snow cover in these conditions is inefficient and may result on large errors of the snow cover characterization. Therefore only METOP AVHRR observations are used for mapping snow cover in the Southern Hemisphere. In the current version of the algorithm Antarctica is assumed snow covered all year round, therefore snow cover is not identified and mapped over this continent. In the Northern Hemisphere within the 0 to 25N latitude belt there are no areas with substantial perennial snow cover or areas that receive a sizable amount of seasonal snow cover that could be effectively identified with satellite observations. Therefore at this time this region is assumed snow free all the time and satellite observations over this region are not processed.

In contrast to the Northern Hemisphere where the extent of ice over inland water bodies may be substantial in the Southern Hemisphere ice is confined to the Southern Ocean. Observations in the optical and infrared spectral bands can add little to the snow retrievals in the microwave, therefore in Antarctica ice cover is mapped solely from microwave data.

4.4 GMASI Output Product

The primary output product of the system is the global daily snow and ice map. The map has a simple binary format and is generated on a latitude-longitude grid at about 4 km spatial resolution. The map is continuous, i.e. it does not have gaps due to unavailability of data or inability to perform retrievals. Within the operational system run by NOAA OSDPD, the output product is presented as separate snow and ice maps over Northern and Southern Hemisphere. Within the quasi operational system hosted on NESDIS STAR servers snow/ice maps of the two hemispheres are combined into one global map. Basic characteristics of the GMASI output product are given in Table 4.5. Figure 4.16 presents an example of the daily blended snow and ice map. Table 4.6 provides the key to the coded integers in the GMASI daily snow and ice map.

Links to the GMASI system web pages and data access:

Operational snow and ice maps generated by NOAA OSDPD and NIC

Northern Hemisphere web page

http://satepsanone.nesdis.noaa.gov/northern_hemisphere_multisensor.html

Northern Hemisphere, access to the data (recent week)

<ftp://140.90.213.161/autosnow/4kmNH/>

Southern Hemisphere web page

http://satepsanone.nesdis.noaa.gov/southern_hemisphere_multisensor.html

Southern Hemisphere, access to the data (recent week)

<ftp://140.90.213.161/autosnow/4kmSH/>

Global maps, access to the data (archive)

ftp://www.star.nesdis.noaa.gov/pub/smcd/emb/snow/global_operational_snow_maps/

Quasi-operational snow and ice map images generated by NOAA NESDIS STAR

Global snow and ice maps, web page

http://www.star.nesdis.noaa.gov/smcd/emb/snow/HTML/multisensor_global_snow_ice.html

Global maps, data access

<ftp://www.star.nesdis.noaa.gov/pub/smcd/emb/snow/binary/multisensor/global>

Region	Latitude range	Longitude range	Dimension (columns, lines)	Grid cell size	Parameters derived
Global	90°S - 90° N	180°W – 180°E	9000, 4500	0.04° x 0.04°	Snow, Ice
N. Hemisphere	0°N - 90° N	180°W – 180°E	9000, 2250	0.04° x 0.04°	Snow, Ice
S. Hemisphere	90°S - 0° S	180°W – 180°E	9000, 2250	0.04° x 0.04°	Snow, Ice

Table 4.5 – Characteristics of GMASI daily snow/ice product

Table 4.6 – Interpretation key for GMASI daily snow/ice product

Integer Value	Meaning
0	Open water
1	Land, no snow
2	Snow cover on land
3	Ice on water
20	Open water, ice is not derived
21	Snow-free land, snow is not derived
200 and over	Undetermined

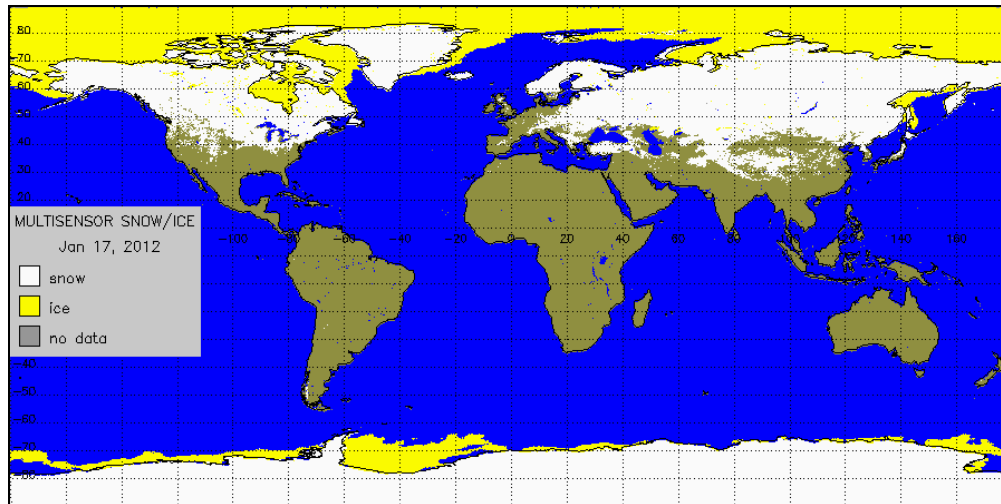


Figure 4.16 – GMASI daily blended snow/ice map

5 GMASI PRODUCT VALIDATION

5.1 Evaluation and Validation Approach

Evaluation and validation of the GMASI product has been performed both qualitatively and quantitatively. Qualitative evaluation included the visual inspection of the maps, their comparison with available satellite false-color and true-color imagery along with the analysis of their consistency with the snow and ice cover climatology and with other remote sensing-based snow and ice products. Quantitative assessment consisted in the detailed comparison of automated snow and ice maps with information on the snow cover provided from ground-based stations and with snow and ice cover mapped interactively within the NOAA IMS system. It is important that only few ground-based stations in the Southern Hemisphere occasionally provide reports on the snow cover on the ground and that the IMS system does not cover areas south of the Equator. Therefore detailed quantitative evaluation of the snow and ice maps can be performed only over the Northern Hemisphere.

5.2 Validation of GMASI Snow Maps

5.2.1 Comparison with in situ data

GMASI snow cover maps are routinely compared to snow cover observations conducted at ground-based meteorological stations. The comparison is limited to the Northern Hemisphere since in the Southern Hemisphere snow cover is observed only at few meteorological station and snow reports are issued quite irregularly. In the Northern Hemisphere information on the snow depth on the ground is reported daily from several thousand meteorological stations the under the auspices of WMO. Additional information on the snow depth may be available from regional in situ observing

networks. In the United States snow depth is routinely observed at several thousand stations within the US Cooperative Network.

It is important that stations under the auspices of the World Meteorological Organization (WMO) do not report “zero” snow depth when there is no snow on the ground. Therefore these reports can be used only to evaluate and assess snow misses in the automated snow maps (or “true positive” accuracy), but not false snow identifications. Stations of the US Cooperative Network do report “zero” snow depth when there is no snow on the ground and thus can be used to calculate all components of the satellite-based snow product error matrix including true and false positives and true and false negatives.

To allow for an easy qualitative evaluation of the consistency of automated snow maps, the system generates daily satellite snow map images with station data overlaid. An example of these maps covering North America and Eurasia is presented in Figure 5.1.

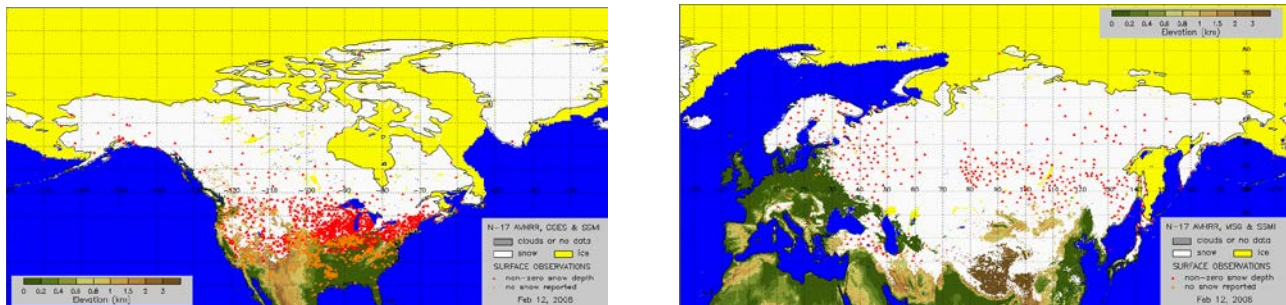


Figure 5.1 – GMSI snow cover maps over North America and Eurasia with surface observations data overlaid. Locations with some snow on the ground are marked with red, stations which reported no snow on the ground are shown in yellow.

Routine quantitative evaluation of the accuracy of snow maps is conducted only over the territory of Conterminous US (CONUS) using snow depth reports from US Cooperative network stations. Availability “zero” snow depth reports from these stations allows for calculation of the complete snow detection accuracy statistics. In the peak of the winter season reports from over 2000 stations may be available for validation of snow maps (see Figure 5.2 for an example of the snow map over CONUS area with station data overlaid).

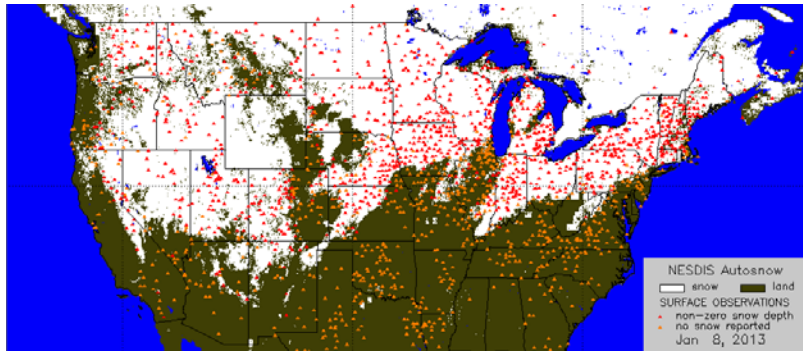


Figure 5.2 – GMASI snow cover over Conterminous US with surface observations data overlaid. Locations with some snow on the ground are marked with red, stations which reported no snow on the ground are shown in yellow.

The comparison of the satellite snow product with station data is performed by matching in situ observation data with the classification status of corresponding grid cells in the snow cover map. The results of the comparison are compiled on a daily basis to estimate the total agreement between the two products. As it is seen from the results presented in Figure 5.3 the daily agreement between the GMASI snow cover and surface snow cover observations changes throughout the year. In late spring, summer, and early fall when the area is mostly snow free the agreement is close to 100%. In middle of the winter season the agreement ranges mostly within 75-85%. Similar seasonal change and similar absolute rates of agreement to surface observations demonstrate NOAA interactive IMS snow cover charts. The yearly mean agreement of automated snow maps to surface observations is 91.4%, which is about 1% below the accuracy of the IMS snow product.

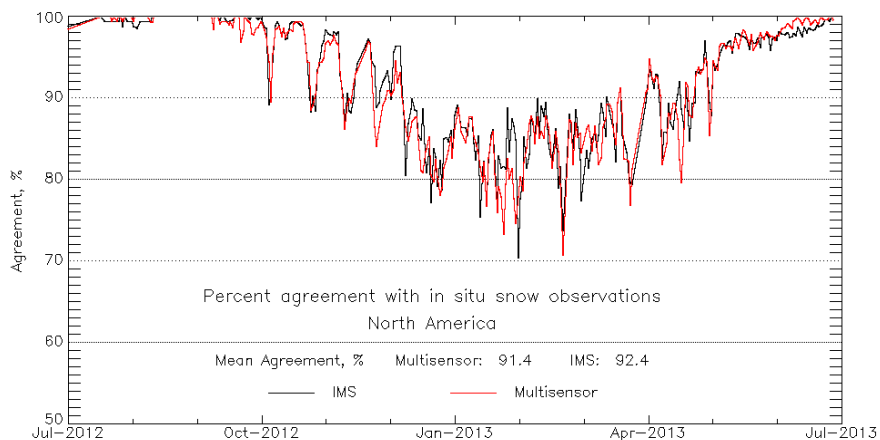


Figure 5.3 – Agreement of GMASI (Multisensor) and IMS snow maps to in situ snow observations over Conterminous US during the time period from July 2012 to July 2013.

5.2.2 Comparison with IMS

Comparison of the automated snow maps with IMS snow products has been performed over Northern Hemisphere. For comparison IMS snow maps were regrided to the 4 km latitude-longitude projection, same as of the automated snow maps. For qualitative evaluation of the agreement between the two products an overlay of the two maps is generated. Figure 5.4 presenting an example of such overlay of the two products demonstrates a good agreement between the automated and the interactive snow cover maps.

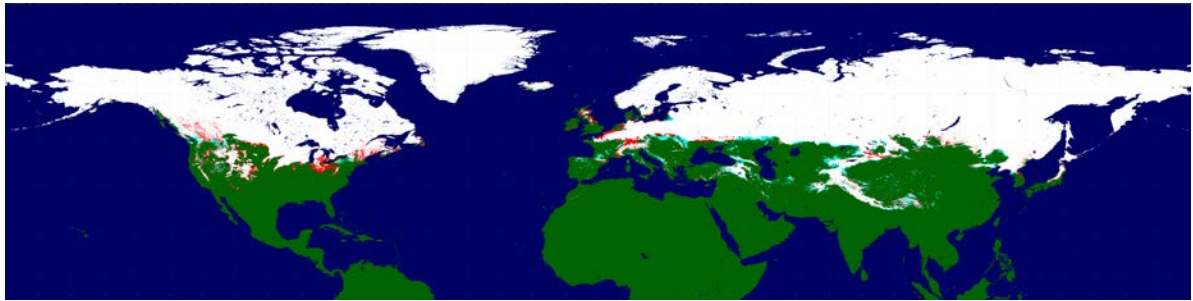


Figure 5.4 – GMASI snow cover map with IMS snow map overlaid. Color codes are as follows, white: both “snow”; green: both “no snow”; red: IMS “snow”, GMASI “no snow; light blue: IMS “no snow”, GMASI “snow”

Quantitative comparison is performed by comparing the two maps pixel-by-pixel. Figure 5.5 presents time series of daily estimates of the percent of correspondence between GMASI snow cover distribution and IMS snow maps over Northern Hemisphere. The mean yearly agreement between the two daily products during the most recent 12-months time period (October 2012 to October 2013) was about 96%. The agreement increases to up to 99% in late summer and decreases to ~93% in the fall and spring season.

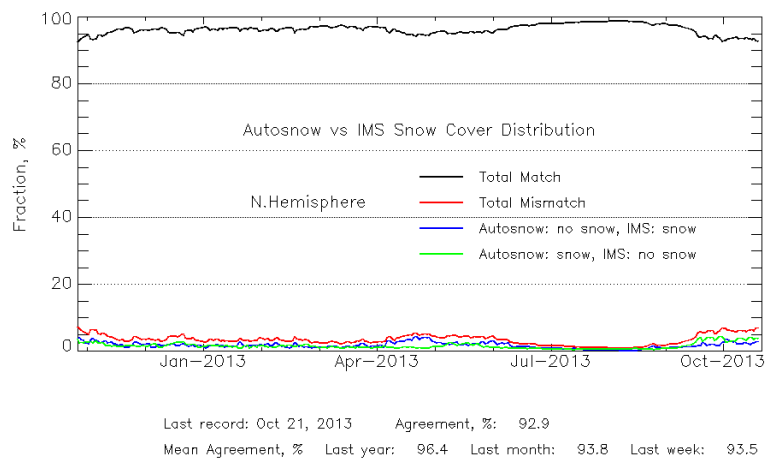


Figure 5.5 – Time series of the rate of agreement/disagreement between GMASI and IMS snow cover distribution for the period from October 2012 to October 2013.

5.3 Validation of GMASI Ice Retrievals

To evaluate the accuracy of ice maps in the Southern Hemisphere we have performed qualitative comparison of the ice cover distribution mapped within the GMASI system with other satellite-based ice cover products over Antarctica generated interactively at NOAA National Ice Center (<http://www.natice.noaa.gov>) and produced by NASA from observations of AMSR-E and SSMIS radiometers (<http://nsidc.org/data/seaice/>). The results of comparison have demonstrated a reasonable performance of the SSMIS ice identification algorithm incorporated in the GMASI system and a close agreement between all products on the ice distribution in Antarctica. Limited quantitative evaluation of the sea ice algorithm performance was conducted by comparing the derived ice extent in the Northern Hemisphere with other ice remote sensing products. The comparison has shown that the difference between the total ice extent generated with the GMASI algorithm and other automated ice extent estimates does not exceed 5%. A larger difference, reaching 8% was found between the Northern Hemisphere ice extent generated with the GMASI algorithm and within the NOAA Interactive Multisensor Snow and Ice Mapping System (IMS). Figure 5.6 presents the time series of daily ice extent estimates in the Northern hemisphere generated with the MASI algorithm and produced from AMSR2 GCOM W1 data at University of Alaska, Fairbanks.

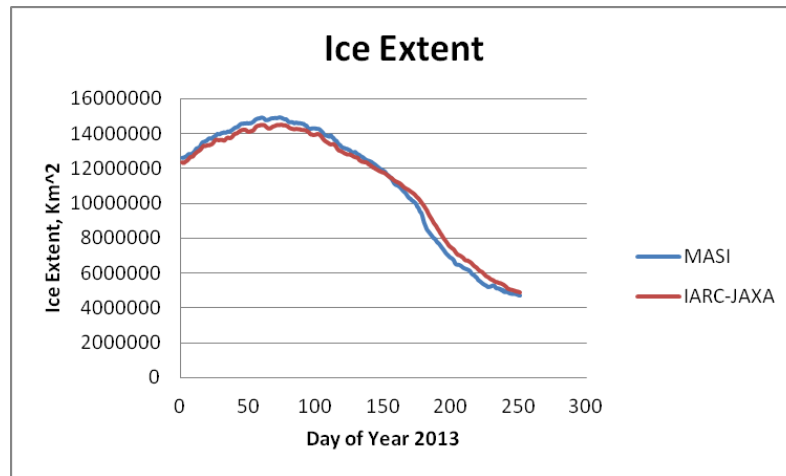


Figure 5.6 – GMASI daily ice extent in Northern Hemisphere and ice extent derived from AMSR2 onboard GCOM-W1 satellite at University of Alaska at Fairbanks (UAF) (http://www.ijis.iarc.uaf.edu/en/home/seaice_extent.htm)

6 ASSUMPTIONS AND LIMITATIONS

6.1 Assumptions

The most essential assumption made in producing global snow and ice cover maps concerns climatic occurrence of the snow and ice cover. Snow/ice is not mapped in the areas that are always snow/ice free or where the extent of snow cover (either perennial or seasonal) is much below the size of the map grid cell. Snow cover is also not mapped over Antarctica which is assumed snow-covered all year round.

6.2 Limitations

The primary limitation of both snow identification techniques, visible/infrared and microwave consists in their inability to identify snow beneath precipitating clouds. As a result quite often a delay of one to several days occurs in mapping fresh-fallen snow. This delay reduces the overall accuracy of snow cover maps and their ability to timely reproduce changes in the snow cover distribution and to identify short-term snow fall-snow melt events. This weakness can be partially compensated by incorporating operational in situ data on the snow cover and/or meteorological radar data. However this latter addition to this system is not planned.

The spatial resolution of satellite observations in the microwave is considerably coarser than of observations in the visible/infrared bands. Therefore, although the nominal spatial resolution of the maps is 4 km, the real spatial resolution makes about 30 km when microwave observations are used to map snow cover or ice. Different spatial resolution of sensors used in the system may cause spurious day-to-day variations in the mapped snow cover.

Snow mapping with observations in the visible and infrared requires sufficient daylight. Early overpass time of METOP (at around 9.30 AM local time) affects the ability to obtain daytime satellite imagery throughout the year in some regions. Most affected is the southern portion of South America mid-latitudes where in the middle of astral winter METOP daytime data may be available only once in three-four days. Unlike the Northern Hemisphere observations in the microwave are not applied for mapping snow in the Southern Hemisphere.

Navigation of METOP AVHRR data is not corrected for topography. In mountainous regions navigation errors due to the parallax effect can exceed 4 km. As a result snow mapped by METOP AVHRR may be misplaced by one grid cell. In rare cases the longitude misplacement may amount to two grid cells.

There are several other limitations of remote sensing techniques affecting the accuracy of snow and ice maps. In particular, topographical and vegetation shadowing of snow hampers proper snow identification with satellite observations in the visible and infrared and may cause snow misses. Dry salt lakes at low, below 15 deg C temperatures produce a spectral response similar to snow in the visible/infrared bands and therefore may be confused with snow cover. The largest permanently or seasonally dry salt lakes are located in the mountainous regions of South America. Melting ice may not be identified properly with the SSMIS observations. This leads to ice misses during the spring season.

6.3 Potential Improvements

- Development and use of finer spatial resolution snow cover climatology
- Development of weekly and/or monthly snow cover statistics
- Replacement of AVHRR with VIIRS data to improve the spatial resolution
- Add AMSR2 onboard GCOM satellite to improve ice mapping
- Add Antarctica snow and ice maps derived with METOP AVHRR data
- Add snow depth and SWE retrievals to create a new layer of product

7 RISKS AND RISK REDUCTION EFFORTS

7.1 Failure of Sensors

As of the time of the last update to this document (October 2013) AVHRR instrument was operating on two METOP satellites –A and –B. The GMASI system can to easily switch from one METOP AVHRR sensor to sensor to another and was tested with both AVHRR instruments. It is highly unlikely that AVHRR sensors on both METOP satellites would fail in the next several years. METOP-C with another AVHRR instrument onboard is scheduled to be launched in 2018.

NPP-Suomi satellite was launched in October 2011. Data from NPP VIIRS became available in early 2012. Due to a different data format, spectral bands, spatial resolution and much larger volume of the data transitioning the retrieval from METOP AVHRR to NPP VIIRS would involve substantial changes to the software. Additional testing of the algorithm performance will be needed since VIIRS spectral response functions in the visible, near infrared and shortwave infrared are different from those of METOP AVHRR.

The GOES system typically includes three satellites, two active, positioned at 135 W (GOES-West), at 75W (GOES-East) and a backup satellite stationed at 100 W longitude. In case of failure, the corresponding satellite will be replaced by the back satellite. Failure of two GOES Imager sensors in a short period of time is unlikely. The first of the new generation of GOES geostationary satellites, GOES-R with the Advanced Baseline Imager (ABI) onboard is scheduled for launch in 2015. Calibration coefficient for the visible band of GOES Imager sensor has to be updated if a new satellite/sensor data are used in the system.

Three Meteosat Second Generation (MSG) satellites carrying SEVIRI instruments are currently on orbit and are stationed at around 0 E longitude. MSG-3 is operational whereas MSG-1 and -2 are in storage. Simultaneous failure of all three instruments is highly unlikely.

SSMIS sensors are currently operating on board of three DMSP satellite, F-16, -17 and -18. In 2014 F-19 is scheduled to be launched. Data available from tree satellites ensures a robust and accurate performance of the ice mapping algorithm. The system, however can properly function with data from two and even one satellite. In the latter case, however, the accuracy of the ice map may decrease since “no ice” identification would become less reliable. It is highly unlikely that all SSMIS sensors fail in the next several years.

7.2 Other problems with satellite data

There is large number of other potential problems with satellite data that may reduce the accuracy of the snow cover product or preclude from generation of snow maps from observation of a particular instrument. These problems include in particular excessive noise, missing scan lines, failing detectors or whole instruments, degraded sensitivity of sensors. It is hardly feasible to foresee all scenarios and to ensure sustainability of the system in all possible adverse situations.

8 LIST OF REFERENCES

- Armstrong, R.L. and M.J. Brodzik (2001) Recent northern hemisphere snow extent: a comparison of data derived from visible and microwave satellite sensors," *Geophysical Research Letters*, 28(19):3673-3676.
- Armstrong, R. L., M..J. Brodzik, M. Savoie, & K. Knowles (2003). Enhanced hemispheric-scale snow mapping through the blending of optical and microwave satellite data. *Geophysical Research Abstracts*, 5, 12824.
- Armstrong R. L., M.J Brodzik, and M Savoie (2004). Enhanced snow cover mapping using combined optical and passive microwave data. *Proceedings of 2004 IEEE International Geoscience and Remote Sensing Symposium*, 20-24 September, 2004, Anchorage, Alaska, CD-ROM.
- Arnell N.W. (1999) Climate change and global water resources, *Global Environmental Change*, 9, S31–S49.
- Baum, B. A., and Q. Trepte, (1999) A grouper threshold approach for scene identification in AVHRR imagery. *J. Atmos. Oceanic Technol.*, 16, 793–800.
- Brasnett, B. (1999) A Global Analysis of Snow Depth for Numerical Weather Prediction. *Journal of Applied Meteorology*, 38, 726–740.
- Cavalieri D.J. (1994) A passive microwave technique for mapping new and young sea ice in seasonal sea ice zones . *Journal of Geophysical Research*, 99, 12561-12572.
- Cavalieri, D. and J. Comiso (2000) Algorithm Theoretical Basis Document for the AMSR-E Sea Ice Algorithm, Landover, Maryland USA: Goddard Space Flight Center.
- Comiso J.C. (1995) SSM/I Sea Ice Concentration using the bootstrap algorithm. NASA Reference Publication 1380, 56.p
- Comiso J.C., D. J. Cavalieri, C. L. Parkinson and P.Gloersen (1997) Passive microwave algorithms for sea ice concentration: A comparison of two technique. *Remote Sensing of Environment*, 60, 357–384.
- C. Derksen , E. LeDrew & B. Goodison (1998) SSM/I derived snow waterequivalent data: The potential for investigating linkages between snow cover and atmospheric circulation, *Atmosphere-Ocean*, 36:2, 95-117.
- SSM/I derived snow water equivalent data: The potential for investigating linkages between snow cover and atmospheric circulation. Available from: https://www.researchgate.net/publication/233310670_SSMI_derived_snow_water_equivalent_data_The_potential_for_investigating_linkages_between_snow_cover_and_atmospheric_circulation [accessed Mar 15, 2016].
- Dery S.J. and R. Brown (2007) Recent Northern Hemisphere snow cover extent trends and implications for the snow-albedo feedback. *Geophysical Research Letters*, 34(22), DOI: 10.1029/2007GL031474
- Drue, C. and G. Heinemann (2005) Accuracy assessment of sea-ice concentrations from MODIS using in-situ measurements. *Remote Sensing of Environment*, 95, 139–149.

- Feijt, Arnout, Paul de Valk, Sibbo van der Veen (2000) Cloud Detection Using Meteosat Imagery and Numerical Weather Prediction Model Data. *J. Appl. Meteor.*, **39**, 1017–1030.
- Foster J.L., D. K. Hall, J. B. Eylander, G. A. Riggs, S. V. Nghiem, M. Tedesco, E. Kim, P.M. Montesano, R. E. J. Kelly, K. A. Casey and B. Choudhury (2011) A blended global snow product using visible, passive microwave and scatterometer satellite data. *International Journal of Remote Sensing*, **32**, 1371-1395
- Gao Y., H. Xie, N. Lu, T. Yao and T. Liang (2010) Toward advanced daily cloud-free snow cover and snow water equivalent products from Terra–Aqua MODIS and Aqua AMSR-E measurements. *Journal of Hydrology*, **385**, 23–35.
- Grody N.C (1991) Classification of snow cover and precipitation using the Special Sensor Microwave Imager. *Journal of Geophysical Research*, **96**, 7423–7435.
- Grody N.C. and A. N. Basist (1996) Global identification of snowcover using SSM/I measurements. *IEEE Transactions on Geoscience and Remote Sensing*, **34**, 237–249.
- Hall, D.K., G.A Riggs, J.L. Foster and S.V. Kumar (2010) Development and evaluation of a cloud-gap-filled MODIS daily snow-cover product, *Remote Sensing of Environment*, **114**, 496-503
- Hall, D. K., and G. A. Riggs (2007), Accuracy assessment of the MODIS snow products, *Hydrological Processes*, **21**(12), 1534 – 1547.
- Hall, D.K., J.R. Key, K.A. Casey, G.A. Riggs and D.J. Cavalieri (2004) Sea ice surface temperature product from MODIS. *IEEE Transactions on Geoscience and Remote Sensing*, **42**, 1076–1087.
- Hsu, N. C., Tsay, S.-C., King, M. D., and Herman, J. R. (2004). Aerosol Properties Over Bright-Reflecting Source Regions, *IEEE Transactions on Geoscience and Remote Sensing*, **42**, 557–569.
- Hyvarinen, O., K. Eerola, N. Siljamo, and J. Koskinen, (2009) Comparison of snow cover from satellite and numerical weather prediction models in Northern Hemisphere and northern Europe. *Journal of Applied Meteorology and Climatology*, **48**, 1199–1216.
- R. E. Kelly, A. T. Chang, L. Tsang, and J. L. Foster (2003) A prototype AMSR-E global snow area and snow depth algorithm, *IEEE Trans. Geosci. Remote Sensing*, vol. **41**, pp. 230–242.
- Key, J.R., X.J. Wang, J.C. Stroeve. and C.Fowler (2001) Estimating the cloudy-sky albedo of sea ice and snow from space. *Journal of Geophysical Research – Atmospheres*, **106**, 12489–12497.
- Kongoli, C., C. Dean, S. Helfrich, and R. Ferraro (2007). Estimating the potential of a blended passive microwave-interactive multi-sensor snow water equivalent product for improved mapping of snow cover and estimations of snow water equivalent. *Hydrological Processes*, **21**:1597-1607.
- Kongoli, C. S.A. Boukabara, S.-A., B. Yan, F. Weng, R. Ferraro, R. (2011) A New Sea-Ice Concentration Algorithm Based on Microwave Surface Emissivities—Application to AMSU Measurements. *IEEE Transactions on Geoscience and Remote Sensing*, **49**, 175 – 189.
- Latifovic R and D Pouliot (2007). Analysis of climate change impacts on lake ice phenology in Canada using the historical satellite data record. *Remote Sensing of Environment* **106**, 492-507
- Liang T., X. Huang, C. Wu, X. Liu, W. Li and Z.Guo (2008) Application of MODIS data on snow cover monitoring in pastoral area: A case study in the Northern Xianjiang, China. *Remote Sensing of Environment*, **112**, 1514-1526.

- Loyola D.G., M. E. Koukouli, P. Valks, D. S. Balis, N. Hao, M. Van Roozendaal, R. J. D. Spurr, W. Zimmer, S. Kiemle, C. Lerot and J.-C. Lambert (2011) The GOME-2 total column ozone product: Retrieval algorithm and ground-based validation. *Journal of Geophysical Research*, 116(D7), DOI: 10.1029/2010JD014675
- Pullen S., C. Jones and G. Rooney (2011) Using satellite-derived snow cover data to implement a snow analysis in the met office NWP model. *Journal of Applied Meteorology*, 50, 958–973.
- Romanov P., G. Gutman and I. Csiszar (2000) Automated monitoring of snow cover over North America with multispectral satellite data, *Journal of applied Meteorology*, 39, 1866-1880.
- Romanov P, Tarpley D (2006). Monitoring snow cover over Europe with Meteosat SEVIRI. *Proceedings of the 2005 EUMETSAT Meteorological Satellite Conference*, 282–287.
- Royer, A., Goïta, K., Kohn, J., DeSève, D. (2010) Monitoring dry, wet and no-snow conditions from microwave satellite observations. *IEEE Geosciences Remote Sensing Letters* 7, 670–674. doi:10.1109/LGRS.2010.2045733.
- de Wildt M, G. Seiz, A. Gruen, (2007). Operational snow mapping using multitemporal Meteosat SEVIRI imagery, *Remote Sensing of Environment*, 109:29-41.
- Pascal S., R. Mathieu, and Y. Arnaud (2009), Subpixel monitoring of the seasonal snow cover with MODIS at 250 m spatial resolution in the Southern Alps of New Zealand: Methodology and accuracy assessment, *Remote Sens. Environ.*, 113(1), 160–181.
- Riggs, G.A., D.K. Hall and S.A. Ackerman (1999) Sea ice extent and classification mapping with the moderate resolution imaging spectroradiometer airborne simulator. *Remote Sensing of Environment*, 68, 152–163.
- Robinson D. A. and G. Kukla (1985) Maximum surface albedo of seasonally snow-covered lands in the Northern Hemisphere. *Journal of Climate and Applied Meteorology*, 24, 402-411.
- Tang Q. and D. P. Lettenmaier (2010) Use of satellite snow-cover data for streamflow prediction in the Feather River Basin, California. *International Journal of Remote Sensing*. 31, Issue 14, 2010, 3745-3762.
- Tedesco M. and J. R. Wang (2006) Atmospheric correction of AMSR-E brightness temperatures for dry snow cover mapping, *IEEE Geosci. Remote Sens. Lett.*, vol. 3, no. 3, pp. 320–324.
- Wang X. and J.R. Key (2001), Spatial variability of the sea-ice radiation budget and its effect on aggregate-area fluxes. *Annals of Glaciology*, 33, 248–252.
- Wang X. and Key, J.R. (2005), Arctic surface, cloud, and radiation properties based on the AVHRR Polar Pathfinder dataset. Part II. Recent trends. *Journal of Climate*, 18, 2575–2593.
- Yan, B., & Weng, F. (2008). Intercalibration between Special Sensor Microwave Imager/Sounder and Special Sensor Microwave Imager. *Geoscience and Remote Sensing, IEEE Transactions on*, 46(4), 984-995.
- Zibordi G. and M.L. Vanwoert, (1993) Antarctic sea ice mapping using the AVHRR. *Remote Sensing of Environment*, 45, pp. 155–163.
- Zibordi G., M.L. Vanwoert,, G.P. Meloni and I. Canossi (1995) Intercomparisons of sea ice concentration from SSM/I and AVHRR data of the Ross Sea. *Remote Sensing of Environment*, 53, p. 145.

END OF DOCUMENT